Marlene Turner, BSc

Design study of a low-energy extension of the H8 beam-line at the CERN Super Proton Synchrotron

MASTER THESIS

For obtaining the academic degree
Diplom-Ingenieur

Master Programme of
Technical Physics

TU Graz

Graz University of Technology

Graz University of Technology

Supervisor:

Assoc.Prof. Dipl.-Phys. Dr.rer.nat. Wolfgang Sprengel

Institute of Materials Physics

Graz, May 2014

EIDESSTATTLICHE ERKLÄRUNG

AFFIDAVIT

Ich erkläre an Eides statt, dass ich die vorliegende Arbeit selbstständig verfasst, andere als die angegebenen Quellen/Hilfsmittel nicht benutzt, und die den benutzten Quellen wörtlich und inhaltlich entnommenen Stellen als solche kenntlich gemacht habe. Das in TUGRAZonline hochgeladene Textdokument ist mit der vorliegenden Masterarbeit identisch.

I declare that I have authored this thesis independently, that I have not used other than the declared sources/resources, and that I have explicitly indicated all material which has been quoted either literally or by content from the sources used. The text document uploaded to TUGRAZonline is identical to the present master's thesis.

_____   _____
Datum / Date   Unterschrift / Signature

Acknowledgement:

I would like to express my special appreciation and thanks to CERN and my supervisor **Ilias Efthymiopoulos** for giving me the possibility to write my Master Thesis at CERN in Geneva, Switzerland. Furthermore, I want to thank him for encouraging my research and for allowing me to grow as a research scientist. His advice on both research as well as on my career have been exceptional. The work was supported by the AIDA, EC/FP7 Grant Agreement 262025.

Even though I have not had the opportunity to work directly with **Lau Gatignon** (CERN), the impact of his help and advice on my own study is obvious throughout this thesis.

Moreover, I have to thank my supervisor at the TU Graz Prof. **Wolfgang Sprengel**. Without his assistance and dedicated involvement, this thesis would have never been possible. I would like to thank for his support and understanding.

Getting through university required more than academic support, and I have many people to thank for listening to and, at times, having to tolerate me over the past five years. I cannot begin to express my gratitude and appreciation for their friendship. Lisa Marx and Barbara Geier, have been unwavering in their personal and professional support during the time I spent at the University. For many memorable evenings out and in, I must thank everyone above as well as Manuel Zingl, Gernot Kraberger, Patrick Falk, Martin Kupper, Paul Christian, Georg Urstöger, Christian Röthel, Christian Neubauer, Oliver Hiden, Katharina Pirsch, Yisel Martinez Palenzuela and Harald Fitzek.

Most importantly, none of this could have happened without my family. My mother and father, who offered their permanent encouragement. It would be an understatement to say that, as a family, we have experienced some ups and downs in the past five years. Every time I needed some support they gave it to me and I am forever grateful. This thesis stands as a testimony to your unconditional love and encouragement.

Contents

Abstract

Design study of a new low-energy beam in the H8 beam-line of CERN SPS to provide 1 to 9 GeV/c electrons, pion and muons. Two layout configurations are considered. Layout 1 brings the beam back to the central line after the particle selection. In layout 2 the beam at the experiment is off-axis. Studies of particle rates with optimized magnet settings and optics studies for beam transmission and focusing to experiment were performed. FLUKA simulations of all beam-line options were made to estimate the spot-sizes, the particle rates and the backgrounds at the experiments. The results showed that the background is significantly lower in layout 2.

Kurzfassung

Für die CERN SPS H8 beam-line wurde eine neue niederenergetischen Teilchen-strahlerweiterung designed und simuliert. Dieser Erweiterung ermöglicht die Bereitstellung von Elektronen, Pionen und Myonen in einem Energiebereich von 1 bis 9 GeV/c. Zwei verschiedene Layout-Konfigurationen wurden getestet. Layout 1 bringt den Strahl nach der Teilchenselektion wieder zurück auf die die Strahl-Mittellinie, während der Strahl in Layout 2 die Mittellinie zum Experiment hin schräg überkreuzt. Die Teilchenraten wurden für verschiedene Magnet-Einstellungen gemessen und optimiert. Strahloptik-Studien für den Strahltransport und die Strahl-fokussierung am Experiment wurden durchgeführt. FLUKA Simulationen zu allen Layout-Optionen wurden ausgeführt um den Strahldurchmesser, die Teilchenraten und Hintergrundevents am Experiment abzuschätzen. Die Ergebnisse zeigten, dass die Hintergrundevents für Layout 2 signifikant geringer sind.

1   Introduction

The H8 beam-line of CERN SPS (Super-Proton-Synchrotron) is located in the experimental hall north (North Area, EHN1) on the Prevessin site. The same hall hosts several beam-lines ($H2, H4, H6, H8$) and many different experiments. The H8 beam-line presently provides 10-350 GeV/c muon, pion or electron beams. For testing the prototype MIND and TASD detectors a tertiary beam extension of the beam-line is needed to provide optimized beams of electrons (e^-), pions (π) and muons (μ) in the low-energy range of 1-9 GeV.

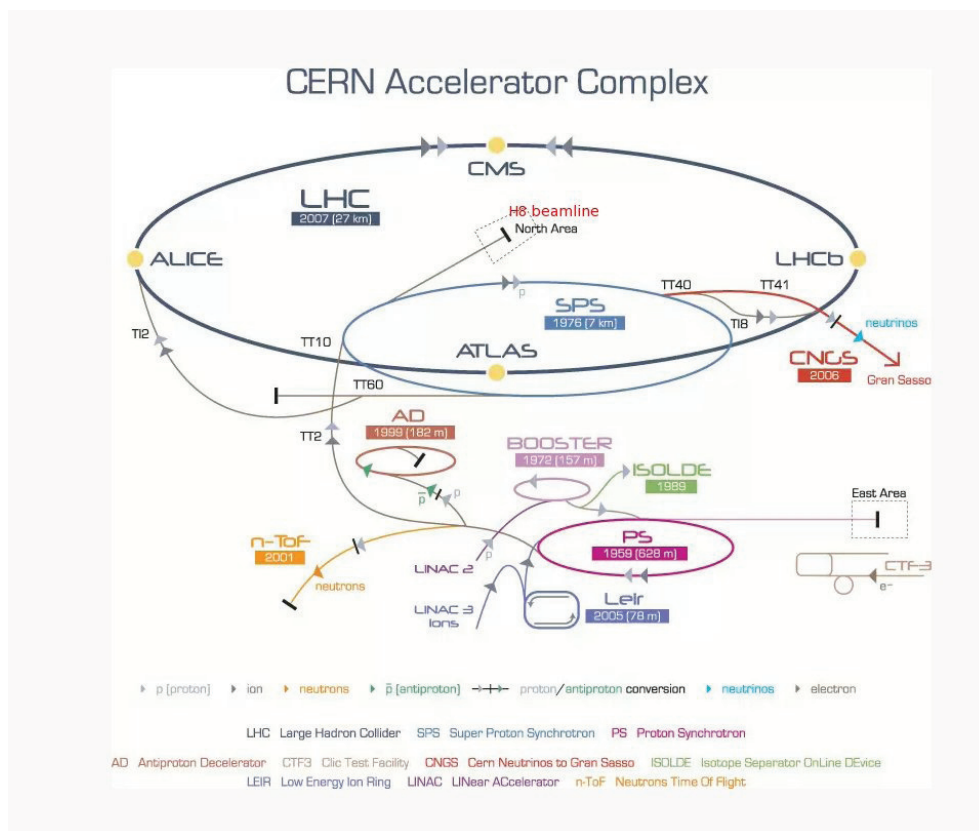## 1.1   The CERN Accelerator Complex

Figure 1: Layout of the CERN Accelerator Complex. The H8 beam-line is located in the North Area. [2]

After extracting the 400 GeV/c primary proton beam from the SPS, bunches of 10^{13} protons hit the primary target (T4) producing a secondary hadron beam. The H8 secondary beam has an energy range from

20-350 GeV, and can transport electrons, muons and pions to the EHN1 experimental hall.

The particle transport and focusing is controlled with magnetic fields. Quadrupole Magnets are used for focusing and defocussing, while dipole magnets are used for bending the beam in an angle. A spectrometer system combined with two collimators is used for momentum selection. For the design, simulation and calculation of the beam-line the programs Transport [3], Turtle [4], HALO [5] and Fluka [6] are used.

Figure 2: View of the H8 and other beam-lines emerging from the primary (T4) target located at the North Area test beam facility. [7]

1.2 Goal

The goal of this Master's thesis is to design a system capable of providing low-energy muon, pion and electron beams employing the H8 beam-line in an energy range from 1-9 GeV/c by improving the existing very-low energy extension used in the past experiments.

The main tasks include:

- Design of the optics for the very-low energy muon, pion and electron beam. Decide how many and which magnets should be used for transportation and selection.

- Minimize the background (unwanted particles from halo and pion-decay) at the experiment. Testing of different design options.

- Maximize the acceptance of the beam-line. Varying of quadrupole magnet positions and magnet apertures.

- Maximize the μ/π ratio at the experiment and optimize the purity of the low-energy muon beam. Select low-energy muons as effectively as possible whilst rejecting other particles and muons outside the energy range.

- Optimize the target size and material for pion,muon and electron production.

- Adapt to the layout constraints in the building. Use of the large Morpurgo magnet.

2   Beam Design Principles

There are various individual steps that must be considered while designing and building a particle beam.

- The particle production - how to produce the desired particles from the primary beam of the preceding section.

- Beam preparation and transport - initial focusing and transport of the produced particles through all magnets and elements.

- Particle selection - deflection of unwanted particles or particles with incorrect energy from the central beam-line.

- Final focusing to the experiments - ensure to get the requested spot size and intensity at the experiment.

2.1   Particle Production

Protons interacting with a target produce directly particles of different types,

$$p, \bar{p}, \pi^{\pm}, K^{\pm}, \mu^{\pm}, e, \gamma, K^0, \Lambda^0.$$

Amongst all the elementary charged particles, the ones of principal interest are listed in Fig. 3 together with their most important characteristics.

Figure 3: Chart of particles and their most important characteristics. [7]

The mass, mean lifetime and decay distance listed in Fig. 3 hold for particles with $v \ll c$. If the particles are moving at a speed close to the speed of light c, special relativity corrections in the laboratory frame have to be made according to: [8]
(τ_0, m_0 for a particle at rest)

Lifetime:

$$\tau = \frac{\tau_0}{\sqrt{1 - \beta^2}} \tag{1}$$

Mean decay distance:

$$l_d = \frac{\beta c}{\sqrt{1 - \beta^2}} \tau_0 \tag{2}$$

Mass:

$$m = \frac{m_0}{\sqrt{1 - \beta^2}} \tag{3}$$

with:

$$\beta \equiv \frac{v}{c} \tag{4}$$

and c the velocity of light For indirect muon production pions ($\pi^{\pm}$) are most interesting because they decay into muons and neutrinos. Also Kaons decay the same way, but the rate of Kaons is negligible:

$$\pi^+ (or \ K^+) \rightarrow \mu^+ + \bar{\nu} \tag{5}$$

$$\pi^- (or \ K^-) \rightarrow \mu^- + \nu \tag{6}$$

After the decay the produced muons carry 57- to 100% of the $\pi^{\pm}$ and 0-100 % of the $K^{\pm}$ initial energy.

Interactions with matter:

Since all the particles of interest carry an electric charge they are affected by the electro-magnetic field produced by the magnets.

$$\frac{d(m\bar{v})}{dt} = e(\bar{E} + \bar{v} \times \bar{B}) \tag{7}$$

When traversing matter the beam particles may interact with orbital electrons and atomic nuclei, in the target, and elastic or inelastic scattering occurs. The most important effects are: ionization of atoms, multiple Coulomb scattering and Bremsstrahlung. Hadrons (like the $\pi^{\pm}$, p and $K^{\pm}$) can also have strong, nuclear and electromagnetic interactions while leptons ($e^-, \mu^{\pm}$) interact through the electromagnetic and weak force. [8]

The choice of target material and size is influenced by:

1) The fraction of the particles required to interact.
2) The type of primary and secondary particles required.
3) Primary beam intensity and the corresponding heat dissipation.
4) Preferred energy of the secondary beam.

Typical target materials are beryllium, copper, carbon and lead.

The secondary meson production per $\frac{GeV}{c}.sterad$ can be approximated for small targets with:

$$\frac{d^2N}{dpd\Omega} = A[\frac{B}{p_0}e^{\frac{-Bp}{p_0}}][\frac{Cp^2}{\pi}e^{-C(p\theta)^2}], \tag{8}$$

Table 1: Empirically derived coefficients A,B,C i.e. for beryllium: [8]

Particle Type	A	B	C
π^-	0.8	11.5	5.0
π^+	1.2	9.5	5.0
K^-	0.1	13.0	3.5
K^+	0.16	8.5	3.0

Table 2: Main characteristics of the available magnets for the VLE beam.

Name	Max BL/T	B at tip/kG	Length/m	A/mm	I_{max}/A	R/Ω
QPL	22.4	11.2	2.0	200	750	205.0
QPS	12.2	12.2	1.0	200	750	205.5
MBPL	3.8	2.0	110-200		850	208

2.2   Beam Preparation and Transport

2.2.1   Main elements of the beam-line

The main elements of the beam-line are listed in Tab. 2. Max BL is the maximum value of the length multiplied with the magnetic field in Tesla·meter, 'B at tip' gives the magnetic field at the tip of the magnet's pole, l is the total length of the magnet in meters, A is the aperture of the magnet, I_{max} the maximal current with which the magnet can be operated and R the resistance of the magnet.

Quadrupole Magnets: Quadrupole magnets (QUAD, QPL, QPS) are electro-magnets with four poles, two south and two north, opposite to each-other acting as a magnetic lens. This type of magnet is used to focus the beam. A Quadrupole magnet focuses in one plane but defocuses in the other plane. The pole pieces are shaped like hyperboles of the form:

$$xy = \frac{R^2}{2} \tag{9}$$

where R is the inscribed circle radius

With the polarity shown in Fig. 4, the horizontal component of the Lorentz force on a positively charged particle, moving into the plane of the drawing, is directed towards the axis while the vertical component is directed away from the axis. Thus, the magnet focuses horizontally and defocuses vertically. The opposite holds when the current direction, the particle charge or its direction of motion is reversed.

The components of the magnetic field are:

(x,y = position)

$$B_x = -\frac{\partial V}{\partial x} = Gy \tag{10}$$

$$B_y = -\frac{\partial V}{\partial y} = Gx \tag{11}$$
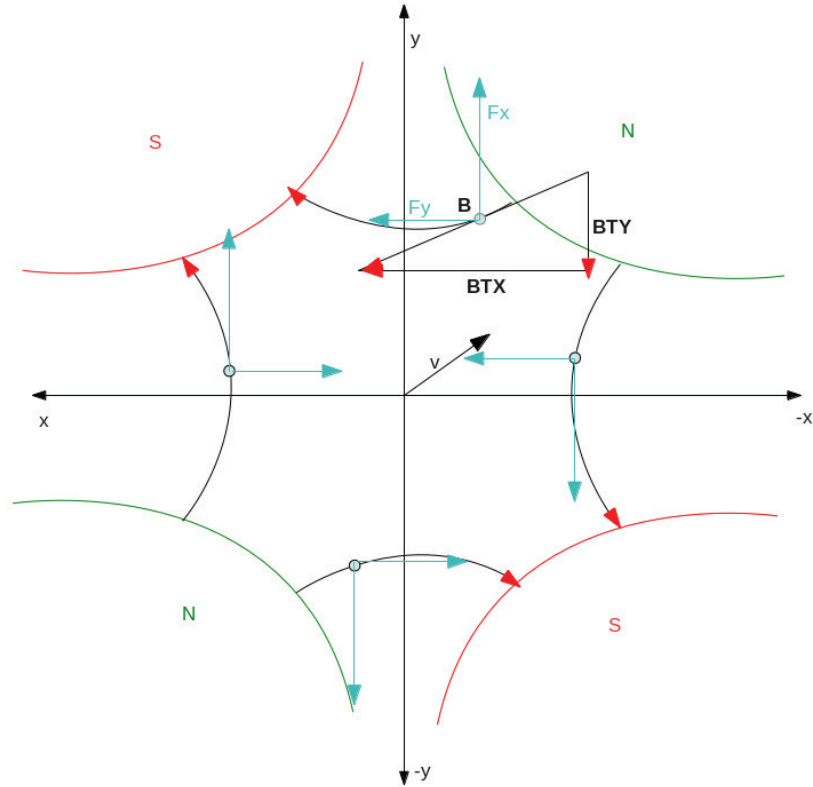
$$B_s = 0 \tag{12}$$

Figure 4: Schematic drawing of a quadrupole magnet. There are two north poles (N) and two south poles (S). B is the magnetic field strength at every point. BTX and BTY are the x and y component of the magnetic field. The curved lines connecting the poles are the magnetic field lines. Fx and Fy are the components of the force that a positively charged particle going in direction $\vec{v}$ sees. [8]

The forces acting on the particles are:

$$F(s, x) = -evB_y = -evGx \tag{13}$$

$$F(s, y) = evB_x = evGy \tag{14}$$

The quadrupole magnets available to use in the new beam-line are called QPL or QPS and have the characteristics listed in Tab. 2. They are chosen due to large aperture.

Dipole Magnets: Dipoles are bending magnets (BEND, MBPL), creating uniform magnetic fields, used in the beam-line to bend the beam with an angle θ. TRIMS are dipole magnets that are used to make small corrections to the beam. Dipole magnets bend and defocus the beam in the plane perpendicular to the magnetic field, the bending plane.
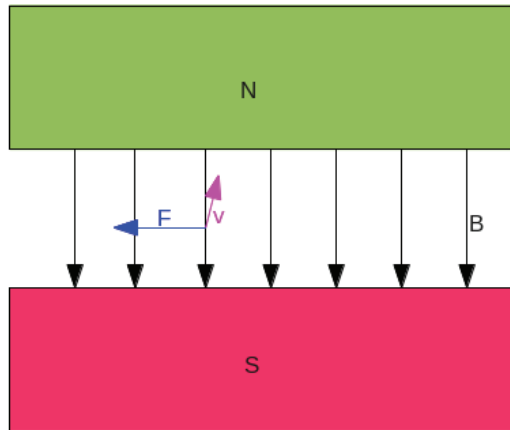
Figure 5: Schematic drawing of a dipole magnet. N is the north, and S the south pole. B are the magnetic field lines. A positively charged particle with direction $\vec{v}$ sees a force $\vec{F}$ ($\vec{F} = q \cdot (\vec{E} + \vec{v} \mathrm{x} \vec{B})$ with $\vec{E} = 0$) perpendicular to $\vec{v}$ and $\vec{B}$. [8]

The deflection angle can be calculated with:

$$\theta = \frac{299.8}{p} Bl \qquad (15)$$

with p in GeV/c, B in Tesla and l the magnetic field length in meters.

The dipole magnets used in the H8 beam-line are called MBPL with the characteristics given in Tab. 2.

2.3 Particle Selection

Muons and pions have to be identified and selected, and all the other unwanted particles (background) have to be rejected.

The momentum selection of the beam-line is determined by a bending magnet (B3) and the acceptance of the following elements in the beam-line, in this example of the VLE Beam another bending magnet (B4) or an optional collimator (COLL). (see Figs. 6 and 7)
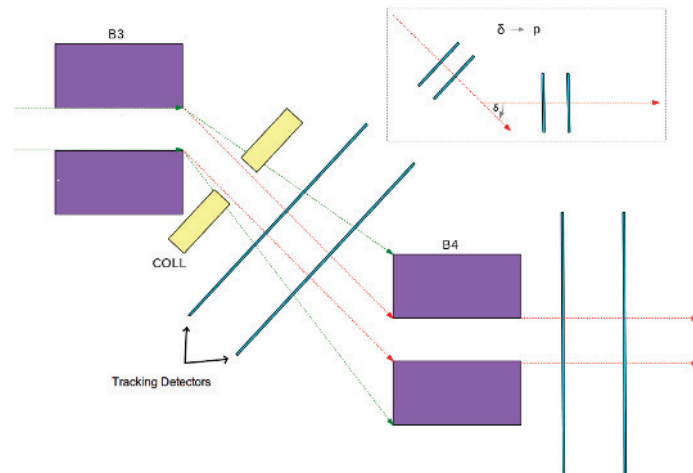
Figure 6: The basic principle of a particle spectrometer. Out of the hits in the tracking detectors the particle path can be reconstructed, the deflection angle calculated and after that, the exact particle momentum determined.
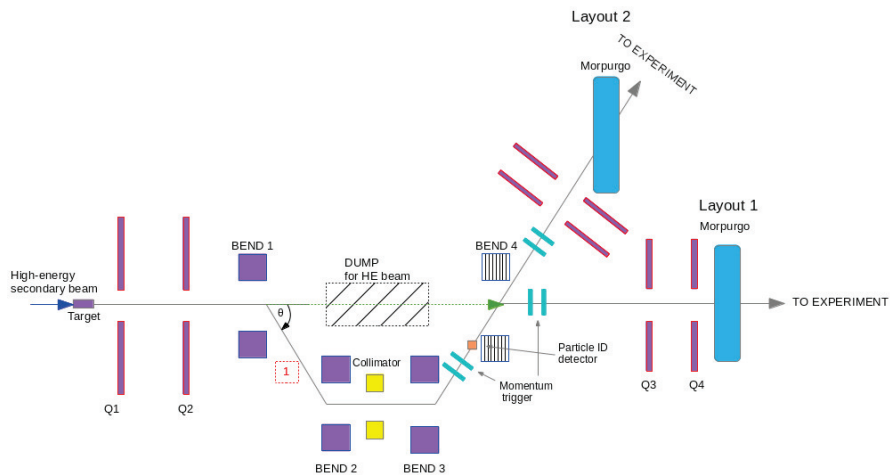

Figure 7: The technique of selecting particles. In this Figure, the two layout options under consideration are combined. This and all other schematic drawings are not to scale. Also see section 2.5 and 2.6.

2.4   Very Low Energy Beam Designs

In the design of this low-energy beam-line, a 20-80 GeV hadron beam hits the secondary target, T48, producing a tertiary hadron beam. Downstream the target two quadrupole magnets are installed, followed in-turn by either three or four bending magnets for momentum selection. At the end, two quadrupole magnets for the final focusing to the experiments are included.

The experiment consists of two detectors. The first one will be placed in the big magnet (Morpurgo) (see Fig. 8 (blue)) and the second one few meters downstream.

The magnetic strengths of all the elements can be set in such a way that the beam-line selects particles from 1-9 GeV. The settings of the magnets will depend on the desired particle type arriving at the experiment. The settings for the beam magnets are listed in Appendix II (section 5).
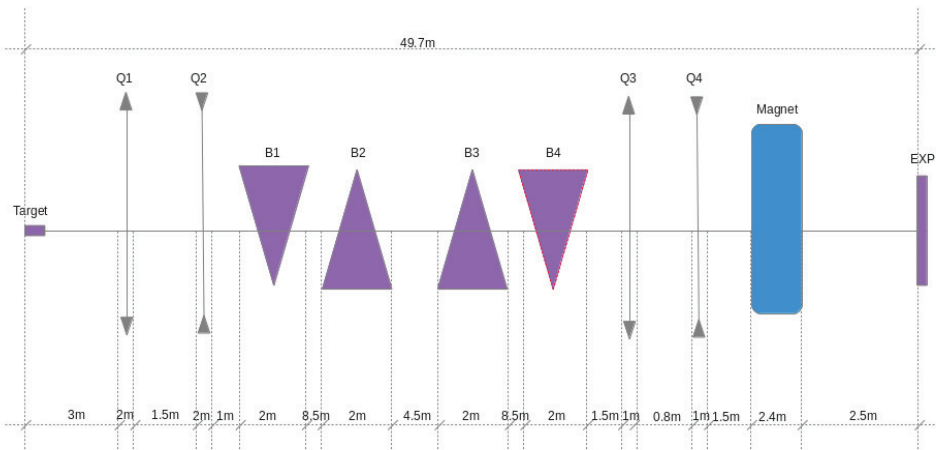

Figure 8: Length of the elements and distance between the elements in the vertical plane.

The positions of all the elements for the designs are as indicated in Fig. 8 (B4 is optional) and Tab. 21 (Appendix II section 5).

The deflection angle is only a bit smaller than the largest possible for the MBPL magnet type, providing 120 mrad of deflection at 1.8 T (see Eq. 16) for the maximum tertiary beam energy of 9 GeV. The maximum $B.L$ = 3.8 T·m (see MBPL Tab. 2). Since the lengths of the MBPL magnets are 2 m, BL = 1.8 T × 2 m = 3.6 T·m.

The strength of the first two bending magnets is calculated out of equation 15 to:

$$p[\text{GeV/c}] = \frac{299.79}{\theta[\text{mrad}]} \cdot \int Bdl[\text{Tm}] \tag{16}$$

In the pion decay the muon will get $57 - 100$ % of the pion momentum because in the π center of mass frame, the pion decays as $\pi \to \mu + \nu$:

$$p_\mu^* = \frac{m_\pi^2 - m_\mu^2}{2m_\pi} = 30 \ \frac{\text{MeV}}{\text{c}} \tag{17}$$

$$E^* = \frac{m_\pi^2 + m_\mu^2}{2m_\pi} = 110 \ \frac{\text{MeV}}{\text{c}} \tag{18}$$

the boost in the laboratory frame gives:

$$E_\mu = \gamma_\pi (E^* + \beta_\pi p^* \cos \theta^*) \tag{19}$$

$$\beta_\pi \approx 1 \tag{20}$$

the limiting cases:

$$\cos(\theta) = +1 \rightarrow E_{max} = 1.0 \ E_\pi \tag{21}$$

$$\cos(\theta) = -1 \rightarrow E_{min} = 0.57 \ E_\pi \tag{22}$$

therefore:

$$\boxed{0.57 \leq \frac{E_\mu}{E_\pi} \leq 1} \tag{23}$$

Because of the results from Eq. 23 the settings of the muon beam for the third and fourth bending magnet are set to 80-85 % of the initial beam momentum. The momentum distributions of the pions and muons look like Figs. 9 and 10 for 6 GeV/c, 9 GeV/c and 15 GeV/c for a pencil beam after 60 m.
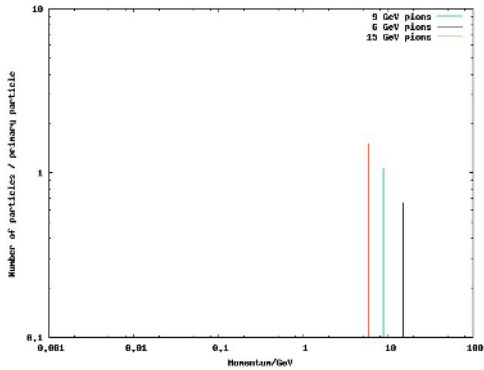

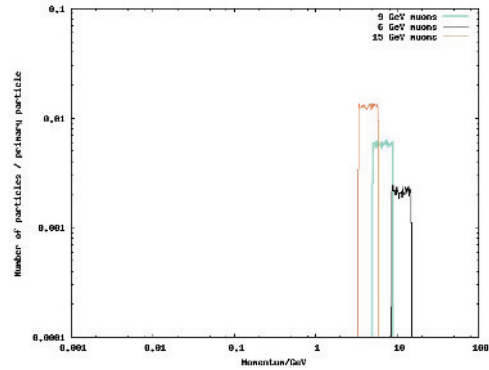Figure 9: Momentum distribution of pions for 6, 9 and 15 GeV/c

Figure 10: Momentum distribution of muons for 6, 9 and 15 GeV/c

2.5 Layout 1

In layout 1 (see Fig. 11) the beam is brought back to the central line downstream the beam dump, that must stop all high energetic particles. However, some remnants and high momentum particles from the secondary beam will go through and reach the experiment. The bending magnets are to be located symmetrically as shown in Fig 11. The setup or the μ beam is:

$$0.8\, B_1 = -0.8\, B_2 = -B_3 = B_4 \tag{24}$$

And for the π or electron beams:

$$B_1 = -B_2 = -B_3 = B_4 \tag{25}$$

Figure 11: Schematic layout of the low-energy extension in the H8 beam-line with 4 bending magnets in the bending (horizontal) plane.

The values of the B fields are shown in Appendix II (section 5, Tab. 17) for pions and muons.

- Advantages:
  - The experiment can receive > 9 GeV beams by removing the beam dump.
  - The detector inside the Morpurgo-Magnet can be placed in a straight and easy way.

- Disadvantages:
  - A large number of unwanted halo particles from high-energy beam travel through the beam dump and arrive at the experiment, because the beam is brought back to the central beam-line.

2.6   Layout 2

Layout 2 (see Fig.12) does not bring the beam back to the central line, therefore no high momentum particles would reach the experiment. Remnant and high momentum particles would arrive with a horizontal displacement of approximately 1 m.

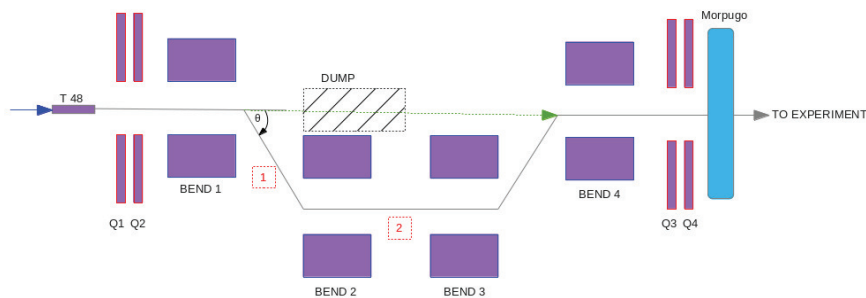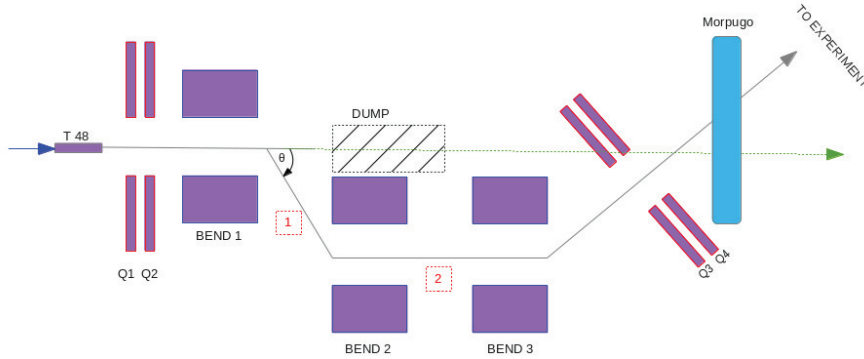Figure 12: Schematic layout of the low-energy extension in the H8 beam-line with 3 bending magnets in the bending (horizontal) plane.

- Advantages:

  - The number of halo particles from the high-energy beam is very much less than in Layout option 1, because the experiment is off-axis. Therefore, a better purity for the low-energy beam can be achieved.

- Disadvantages:

  - The experiment cannot receive high-energy beams > 9 GeV in a simple way.
  - The experiment must be placed in the Morpurgo magnet at an angle.

2.7   Low-Energy Tertiary Beams

This section gives a brief overview of the most important features of each low-energy beam-line.

- For the electron beam:

  - Use a secondary electron beam and a thin secondary lead (Pb) target for optimal low-energy electron production.
  - It is possible to receive a pure low-energy electron beam at the experiment with only very little background.

20

- For the pion beam:

  - A secondary high-energy π, μ, p beam mixture of 80 GeV and a carbon or beryllium target produce a maximum number of low-energy pions.
  - The experiment gets a mixed π and μ beam (There will always be some μ from pion decay after the last selection magnet.)

- For the muon beam:

  - Same as for pions: A secondary high-energy π, μ, p beam mixture of 80 GeV and a carbon or beryllium target is used for muon production.
  - It is possible to tune the magnets to select only low-energy muons.

2.8   Beam Simulation Codes

TRANSPORT

TRANSPORT [3] is a computer program to design a beam-line element-by-element. The elements are inserted with type codes or cards. Every element is assigned and defined by a card. If fitting constraints are inserted, and enough degrees of freedom provided, the program will perform a fit. One has to be very careful that the fitting constraints can be fulfilled with the given degrees of freedom, otherwise the fit will fail. Apart from that, one has to give reasonable starting values for the varied parameters.

TRANSPORT will give a graphical output of the beam-line, tables listing the elements and their corresponding parameters and the beam matrices. TRANSPORT does not take the 3D position of each element, it just takes into account the distance to the next component. Therefore, all magnets are normally considered along the central trajectory. This is a problem for the design of the muon beam and had to be circumvented. In the simple model used here, particles experience a uniform magnetic field which begins and ends abruptly at the entrance and exit faces of the idealized magnet. The process of following a charged particle through a system of magnetic lenses is reduced to a process of matrix multiplication. Thus, the passage through the system may be represented by the equation:

$$X(1) = R(t)X(0) \tag{26}$$

with $X(0)$ the initial coordinate vector, $X(1)$ the final coordinate vector and the transformation matrix $R(t) = R(n)...R(3)R(2)R(1)$.

DECAY-TURTLE

DECAY-TURTLE [4] (hereon referred to as TURTLE) simulates particles
through the beam-line and considers the apertures of the elements. If
particles happen to hit the aperture of an element, they are lost. TUR-
TLE, as well as TRANSPORT, considers all elements aligned on the central
trajectory. TURTLE includes particle decay of the type $1 \rightarrow 2$, following
the parent and two daughter particles through the beam-line. e.g:

$$\pi \rightarrow \mu + \nu \tag{27}$$

As TURTLE [4] and TRANSPORT use the same matrices for their cal-
culations, identical results concerning the beam size and shape at every
position are obtained if the same input parameters and cards are used.

HALO

HALO [5] is a Monte-Carlo computer program which is able to calcu-
late the beam halo particles, i.e. particles outside the vacuum pipe,
which travel with the beam and therefore makes it possible to estimate
the muon background. It is based on the principles contained in TUR-
TLE. The particles are generated by an input beam hitting a hydrogen
target. If a muon leaves the specified central aperture, it is from then on
considered as a halo candidate.

Unlike TRANSPORT and TURTLE, Halo asks for the design momentum
in order to determine the curvature of the reference orbit for each element.

FLUKA

FLUKA [6] is a general purpose tool for calculations of particle transport
and interactions with matter. It implements modern physical models
and enforces conservation laws. The FLUKA hadron-nucleon interaction
models below a few GeV are based on resonance production and decay.
FLUKA carries out its own Monte-Carlo simulations and particle decays
and interactions. It simulates accurately particles hitting the apertures
and the particle production at the target.

In particle tracking, FLUKA differs completely to the previously de-
scribed programs. For the simulation of the magnetic fields, FORTRAN
codes are implemented to create uniform fields for the bending magnets
and simplified magnetic fields for the quadrupole magnets.

One of the main advantages of FLUKA is that one can build the real
geometry. At every point of the beam-line, especially at the end, de-
tectors can be placed. All particles traversing this detector are tracked

and counted and variables of interest are plotted or stored in an output file for further analysis. Data was further processed either directly with FLUKA or ROOT [10].

3   Beam Performance

3.1   Beam Optics

3.1.1   Muon Beam

The Transport simulation was done in two steps. Starting with the simulation of the first part of the beam-line with the initial pion selection momentum until the third bending magnet. Just before the fourth bending magnet, the beam size and the corresponding beam angles are read out and stored. These values are then used as an input beam for the next step of the simulation, where all the elements of the second part of the beam-line are set to the muon momentum ($\approx 80\%$ of the π momentum) making the final focusing to the experiment.
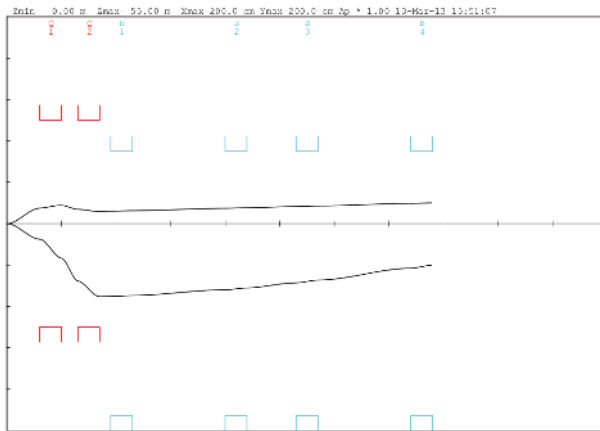

Figure 13: 1st step of the muon beamr Transport simulation. The input beam is point-like and spreads out with an maximum angle of $\pm$ 5 mrad.
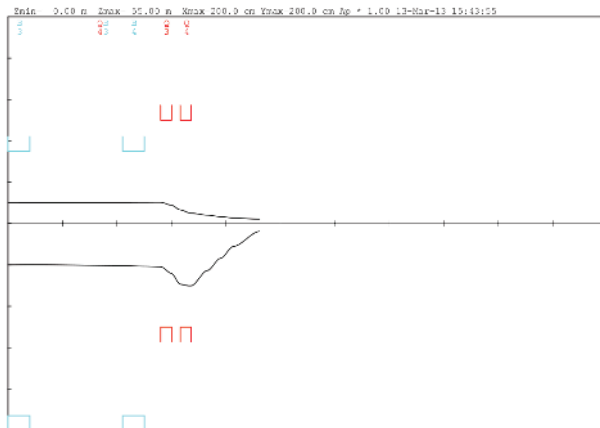

Figure 14: Second step of the VLE muon beam. The input beam parameters used for the simulation are extracted from the first step.

The beam envelope of the VLE muon beam is shown in Figs. 13 and 14. These Figs. show the horizontal (up) and the vertical (down) plane. The red elements are the quadrupole magnets, the turquoise elements are the bending magnets. The green line (only displayed in one-step simulations (Fig. 15, 16)) shows the dispersion. The dipole magnets always bend in the horizontal plane. The output values of the Transport fit for the drift spaces and the magnetic fields are then used as the input values for any further simulations with particles in TURTLE, HALO and FLUKA (see Tab. 18).

3.1.2 Pion Beam

The goal of the VLE pion beam is to transport most pions in the right energy range to the experiments and to keep the number of muons and other particles low. The settings for the magnets are listed in Tabs. 19 and 20. All the elements of the beam-line downstream the secondary target are set to select the desired particle momentum. The geometry and the position of the elements stay the same as for the VLE muon beam. The settings for the magnets are approximately symmetric and the magnetic sequence of the quadrupoles is focusing, defocussing, defocussing, focusing and the other way round in the horizontal plane (see Figs. 15,16). For a beam with a beam sigma of $\sigma = 0.8$ cm a final focusing to $x = \pm\ 2.48$ mm, $y = \pm\ 0.784$ mm is expected at the experiment.
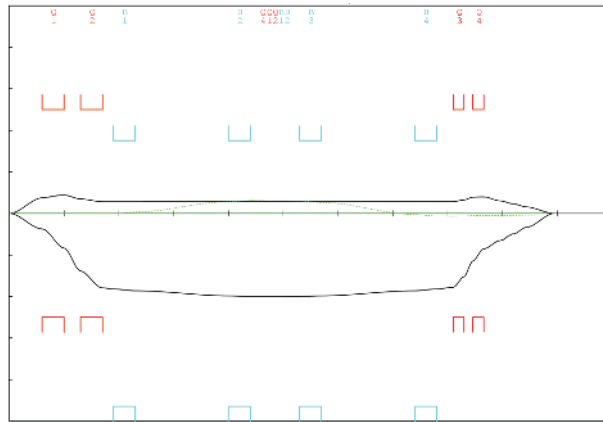

Figure 15: VLE π-beam simulation: Layout 1, Transport simulation of the very-low energy extension. The input beam is point-like and spreads out with an angle of ± 5 mrad.
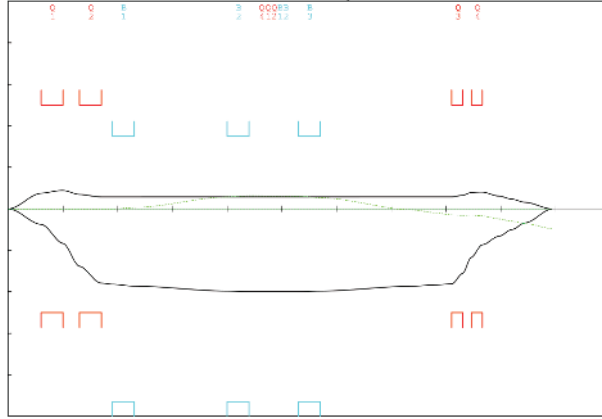
Figure 16: VLE π-beam simulation for Layout 2, same conditions as in Fig. 15

3.1.3 Electron Beam

The main difference between transporting pions and electrons in the VLE beam-line (similarly for electron and positron beam, π^+ and π^- or μ^+ and μ^-) at the same energy is that the muons carry a positive (μ^+) and the electrons (e^-) a negative charge. Therefore, the signs of the magnetic fields of the magnets have to be inverted. Another important difference is that one needs to use a different target for the particle production. (see section 3.1.2)

3.1.4 Acceptance of the Beam-lines

Not all particles coming from a source or a target will make their way through the beam-line. Only particles within a given acceptance will be transported. Particles out of the acceptance range will either not be affected by the magnet fields or hit the apertures. The acceptance is given by different values:

- x... horizontal displacement of the particle with respect to the assumed central trajectory.

- y... vertical displacement of the particle with respect to the assumed central trajectory.

- x'... angle this ray makes in the horizontal plane with respect to the assumed central trajectory.

- y'.. angle this ray makes in the vertical plane with respect to the assumed central trajectory.

- p... momentum of the particle at the source or target.

The theoretical acceptance was measured with TURTLE by using flagged histograms. The flag was put at the end of the beam-line, and the production angle, position and momentum of all the particles arriving at the end are plotted. The results can be seen in Figs. 17 to 21. The values for x and y are given by size of the target or the source. For these simulations the pion beam target with a radius of 2.5 cm was used.

In order to get a high acceptance the first quadrupole magnet is placed close to the secondary target (T48). The beam acceptance simulated with TURTLE for the pion and electron beam with 4 bending magnets is: (see Fig. 17, 18, 19, 20, 21)

Table 3: Acceptance of the very-low energy extension.

x/mm	x'/mrad	y/mm	y'/mrad	p/%
$\approx \pm\, 40$	$\approx \pm\, 7$	$\approx \pm\, 5$	$\approx \pm\, 29$	$\approx \pm 13$

Since the acceptance is mainly determined by the distance and the aperture of first elements of a beam-line, the acceptance for the VLE pion and electron beam-line are similar.
In the following figures, the initial produced particles are shown in black and the accepted particles in red.
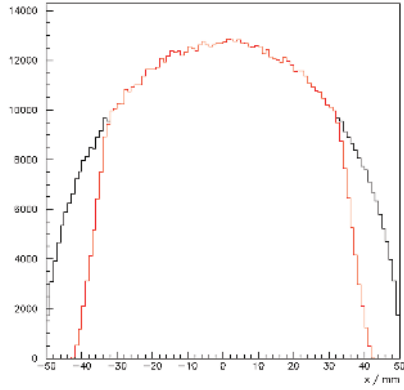
Figure 17: Produced (black) and accepted (red) particles in the horiz. plane as a function of the position of the particles.

Figure 18: Produced (black) and accepted (red) particles as a function of their production angle in the horiz. plane.

Figure 19: Produced (black) and accepted (red) particles in the vert. plane as a function of the position of the particles.

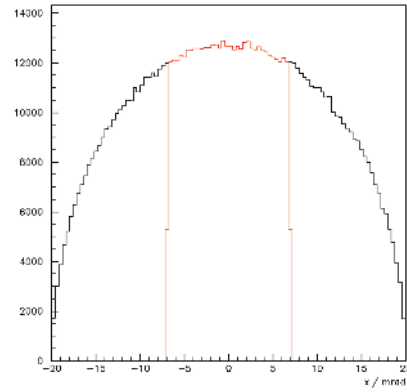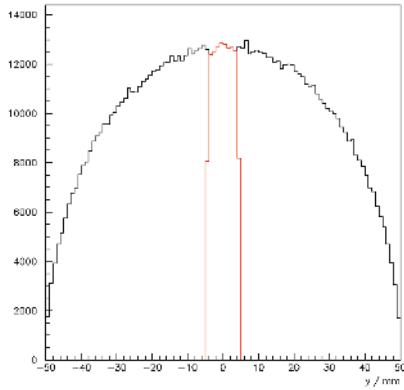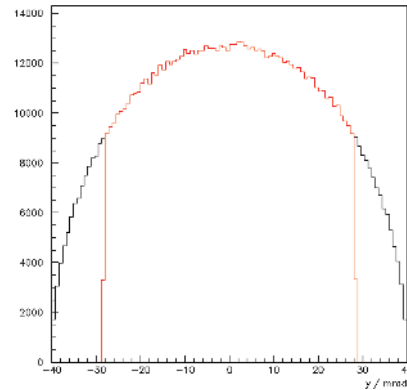Figure 20: Produced (black) and accepted (red) particles as a function of their production angle in the vert. plane.
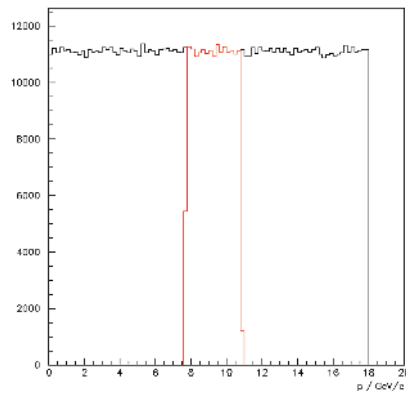

Figure 21: Produced (black) and accepted (red) particles as a function of their initial momentum.

3.1.5 Simulation Tests

Crosschecks of the FLUKA simulation have been made in order to test the simulation and make sure that and especially the magnetic fields of the quadrupole and dipole magnets are working correctly.

Pencil Beam

At the center of a quadrupole magnet ($x = 0, y = 0$) the magnetic field is zero and the beam sees no magnetic field. Hence, if a pencil beam is produced ($\Delta x = 0, \Delta y = 0, \Delta\phi = 0$), the beam should not be affected in any way by the quadrupole magnets (the volume around is filled with vacuum). For the simulation ten-thousand 9 GeV/c primary protons (they do not decay) were used. The settings for a 9 GeV/c pion beam were used. (see Figs. 22 and 23) The figures show the particles arriving in the horizontal and vertical plane at the experiment. All protons arrived at

Figure 22: Spot size in x (horizontal) of the pencil test beam.

Figure 23: Spot size in y (vertical) of the pencil test beam.

the center of the experiment.

If the quadrupole magnets are filled with helium (instead of vacuum) scattering occurs and some of the protons are lost. (see Fig. 24 and 25)
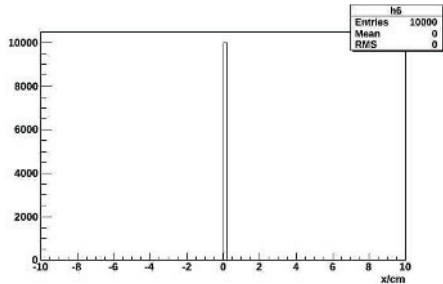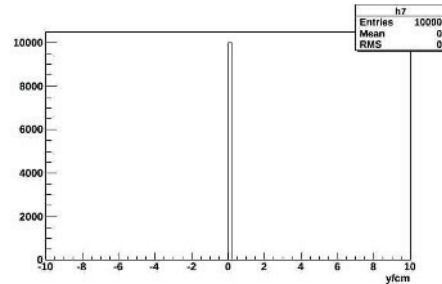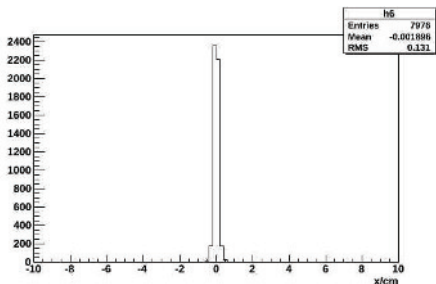

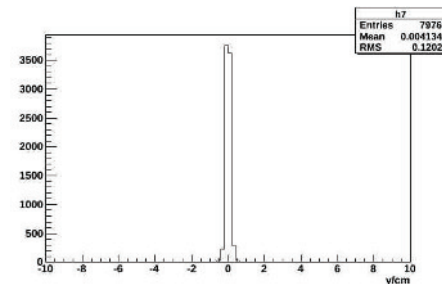Figure 24: Spot size in x (horizontal) of the pencil test beam.

Figure 25: Spot size in y (vertical) of the pencil test beam.

Thin quadrupole magnets

The quadrupole magnets used in the very-low energy extension have a length of one or two meters. In order to test the magnetic field of the quadrupole magnets in the simulation, they were shrinked to a length of one centimeter. The magnetic field strengths were multiplied accordingly. The simulation gave very similar results.

No target

If no target is inserted in the FLUKA simulation the beam shape should be the same as in the Transport simulation. Small variations occur because of the differences in the simulations described in section 2.8.

3.2   Particle Production and Target Study

In order to optimize the target for different particle production simple FLUKA simulations were made. The geometry only consists of the target and a detector around 3 m downstream (see Fig. 26). The detector is a cylinder with a radius of 10 cm (corresponding to the acceptance of the first quadrupole magnet). Only pions or electrons from 1-10 GeV/c are accepted. The target in the simulation has also got a cylindrical shape.

Figure 26: FLUKA geometry for the target study.

The most important characteristic of a target material is the interaction length. The interaction length is different for different kinds of particles. The interaction length for pions is called λ_{int}. For electrons the corresponding value is the radiation length X_0, related to the energy loss of high energy, electromagnetic-interacting particles with the target. The values for λ_{int} and X_0 for different target materials are listed in Tab. 4.

Table 4: Pion and electron interaction length for different materials. [11] λ_{int} is the $\pi-$interaction, and X_0 the radiation length.

Material	λ_{int}/cm	X_0/cm
Beryllium	59.47	35.28
Copper	18.30	1.53
Lead	19.93	0.56
Carbon	58.00	21.35

3.2.1 Target Study for the Pion and Muon Beam

The primary beam for this simulations consists of 4000 primary particles (50 % π^+, 50 % proton). The simulation was simplified by using a pencil beam. First the primary beam momentum was set to of 20 GeV/c (see Fig. 27) and 80 GeV/c (see Fig. 28) and the target length was varied for different materials. The target length in the plots is normalized to the interaction length of the material (given in Tab. 4). The radius of the target in Figs. 27 and 28 is 2.5 cm. Next, the length of the target was fixed and the momentum of the incoming particles and the radius of the target were varied. (see Figs. 29 and 30). The measurements show only particles in a momentum range from 1 to 10 GeV and within the acceptance of the VLE beam extension.
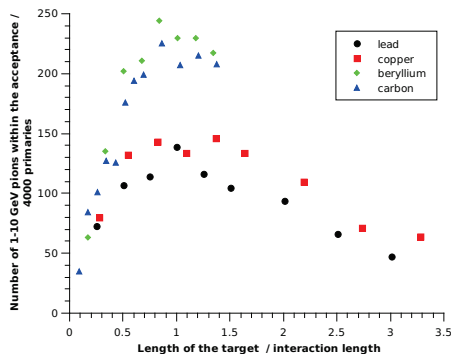
Figure 27: Measured number of pions as a function of the target length. Four different target materials were tested. The momentum of the input beam is 20 GeV/c. The diameter of the target is $\varnothing = 5$ cm

Figure 28: Measured number of pions as a function of the target length. Four different target materials were tested. The momentum of the input beam is 80 GeV/c. The diameter of the target is $\varnothing = 5$ cm

As a result of this simulations a beryllium target with $\approx 1.5\ \lambda_{int}$ (90 cm) and a radius of 0.5 cm would work best for an incoming 80 GeV/c 50% proton 50% π pencil-beam, a copper target of 30 cm will give $\approx 30\%$ less pions.
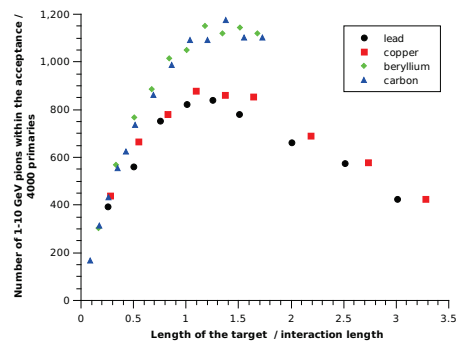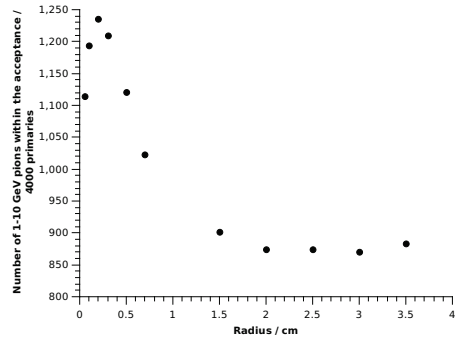
Figure 29: Measured number of pions as a function of the target radius. The momentum of the input beam is 80 GeV/c and the length of the beryllium target is 80 cm.
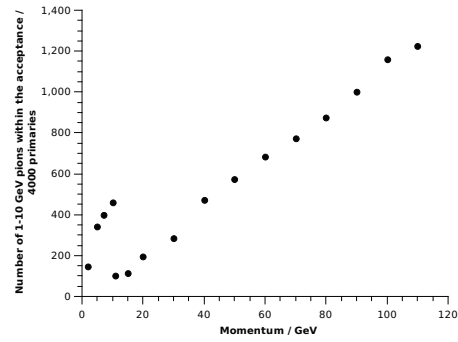
Figure 30: Measured number of pions as a function of the momentum of the incoming particles for a 80 cm beryllium target with a diameter of $\varnothing = 5$cm.

The general trend showed that if the target size is smaller, less particles spray out, therefore more particles are within the acceptance range. And with higher incoming beam momentum, more secondary particles are produced in the target.

3.2.2 Target Study for the Electron Beam

In order to optimize electron production for the VLE electron beam, a primary beam of 4000 primary electrons of 20 and 80 GeV was simulated. Four different targets were tested. The target length is varied, the target radius 0.5 cm maintaining. The results are shown in Figs. 31 to 34.

Figure 31: Number of electrons from 1-10 GeV/c within the acceptance as a function of the target length for different target materials for an input beam of 20 GeV/c. $\varnothing = 0.5$ cm
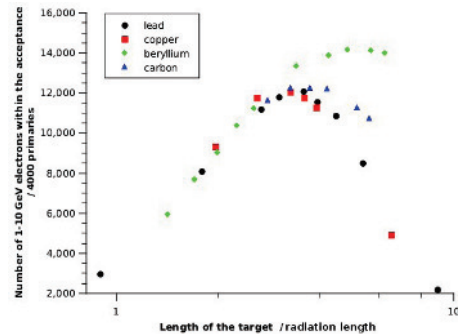
Figure 32: Number of electrons from 1-10 GeV/c within the acceptance as a function of the target length for different target materials for an input beam of 80 GeV/c. $\varnothing = 0.5$ cm
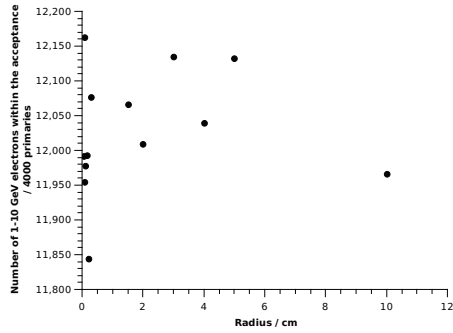
Figure 33: Number of electrons from 1-10 GeV/c within the acceptance as a function of the target radius for an input beam of 80 GeV/c and a 2 cm lead target.

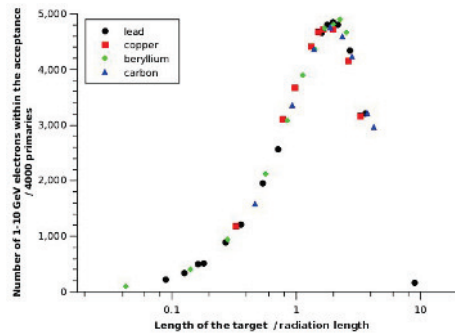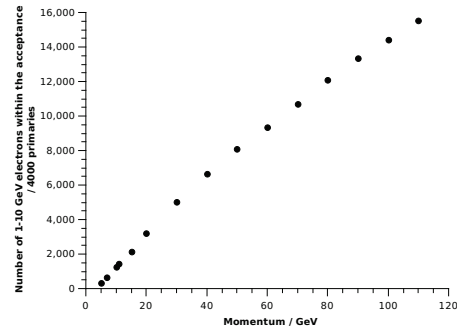Figure 34: Number of electrons from 1-10 GeV/c within the acceptance as a function of the momentum of the incoming particles for a 2 cm beryllium target with $\varnothing = 0.5$ cm.

As can be seen in Fig. 33, there is no preferred radius for a lead target. Any of the four tested target materials with a radiation length of $\approx$ 3-4 would work.

It was decided to use a 2 cm lead target with a radius of 2.5 cm for further simulations with electrons.

3.2.3 Particle Background

When a particle beam hits a target all kind of different particles are produced in a broad momentum range. For example, the secondaries produced by the 80 cm beryllium target with a radius of 0.5 cm by 4000 primary protons of 80 GeV/c are shown in Figs. 35 and 36.

The FLUKA particle ID's are listed in Tab. 5.

Table 5: FLUKA particle ID

Particle	ID	Particle	ID	Particle	ID	Particle	ID
Proton	1	Anti-Proton	2	Electron	3	Positron	4
Neutrino	5	Anti-Neutrino	6	Photon	7	Neutron	8
Anti-Neutron	9	Muon$^+$	10	Muon$^-$	11	KaonLong	12
Pion$^+$	13	Muon$^-$	14	Kaon$^+$	15	Kaon$^-$	16
Lambda	17	Anti-Lambda	18	KaonShort	19	Sigma$^-$	20
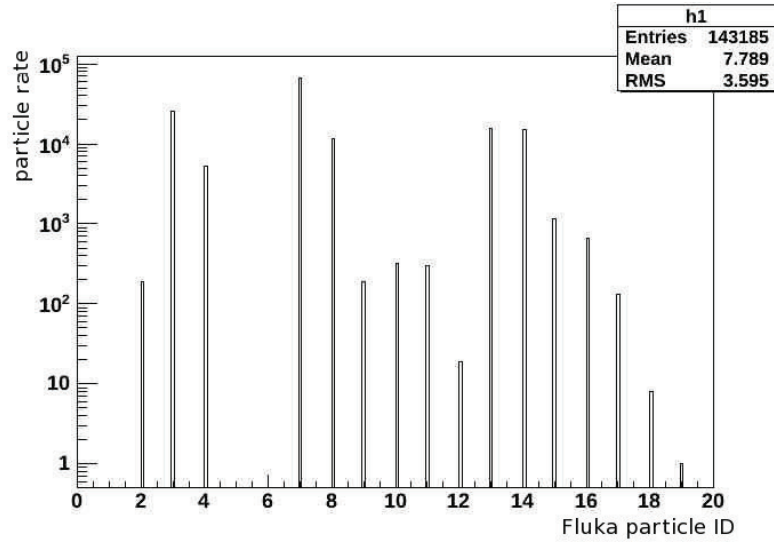
Figure 35: Secondary particles produced at the T48 target beryllium 80 cm 0.5 cm with an 80 GeV proton beam impacting.
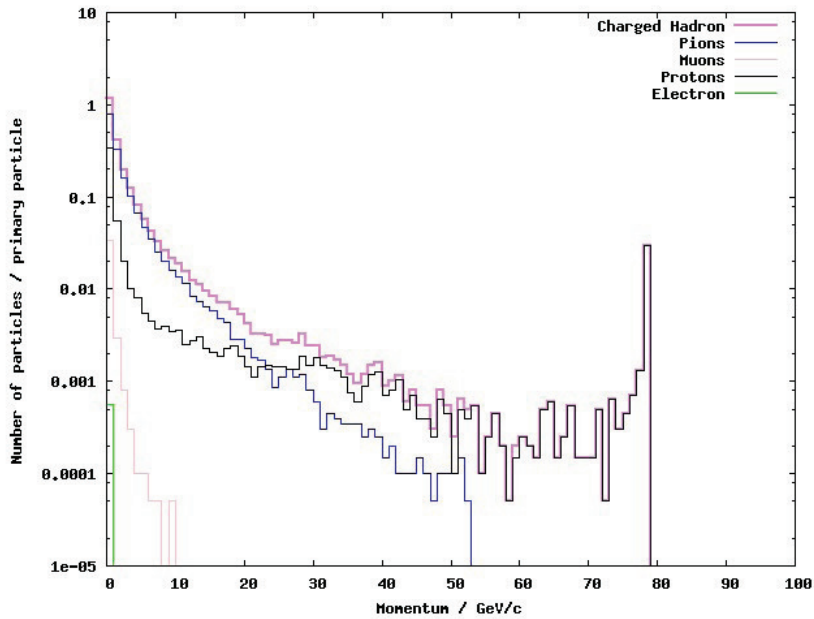
Figure 36: Momentum distribution of the produced secondary particles in Fig. 35

3.3   Muon Beam Optimization

3.3.1   Optimization of the Muon Selection Process

The muon is a decay product of the pion, as already mentioned before:

$$\pi^+ \rightarrow \mu^+ + \bar{\nu} \tag{28}$$

34

Therefore, it is important that the secondary target T48 produces as many π^+ as possible. Pions have an average lifetime of 2.2 ns and go around 55 m/GeV before they decay. The idea of the muon beam-line is such that the first two bends select pions at a certain momentum. Some of those pions will decay (preferably in the region between the second and third bending magnet) and the muons get 57-100 % of the initial pion momentum. The third and the (if used also) fourth bending magnet select the muons at the right momentum. Thus, all the elements following and including the third bend are set to select at an momentum around 80 % of the first part of the beam-line.

The maximum length for the beam-line fitting in the available space in the North Area is around 49.7 m. Both layouts (see Figs. 11,12 and Tab. 21) have a total length of 49.7 m. The maximum possible length was chosen to allow more pions to decay.

For choosing the magnetic settings of elements that select the muons a special FLUKA simulation was made. This simulation uses an initial beam momentum and scales all the elements after a defined point down to the desired muon energy ($\approx 80\%$ of the initial pion energy). The program also scans through the desired muon momentum. The simulation results for 9 GeV/c (selecting muons from 9-7 GeV/c) see Tab. 14, for 6 GeV/c (selecting muons from 6-4 GeV/c) see Tab. 15, 15 GeV/c (selecting muons from 15-13 GeV/c) see Tab. 16. The highlighted line corresponds to 80% of the initial pion momentum.
The values of Tabs. 15 and 14 are plotted in Figs. 37 and 38.
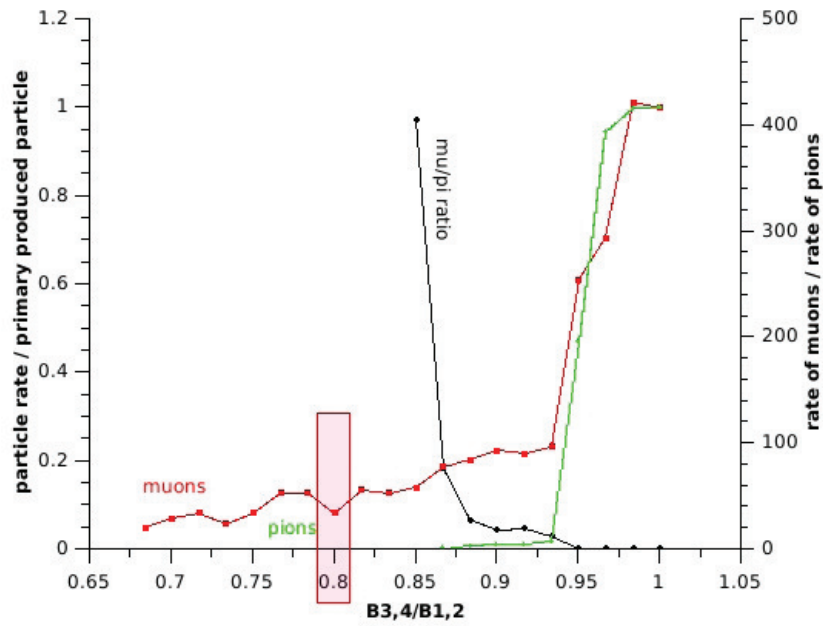
Figure 37: Number of muons μ (red), number of pions π (green), μ/π ratio (black) for 6 GeV/c out of a FLUKA simulation with varying magnet settings for the bending magnets B3 and B4.
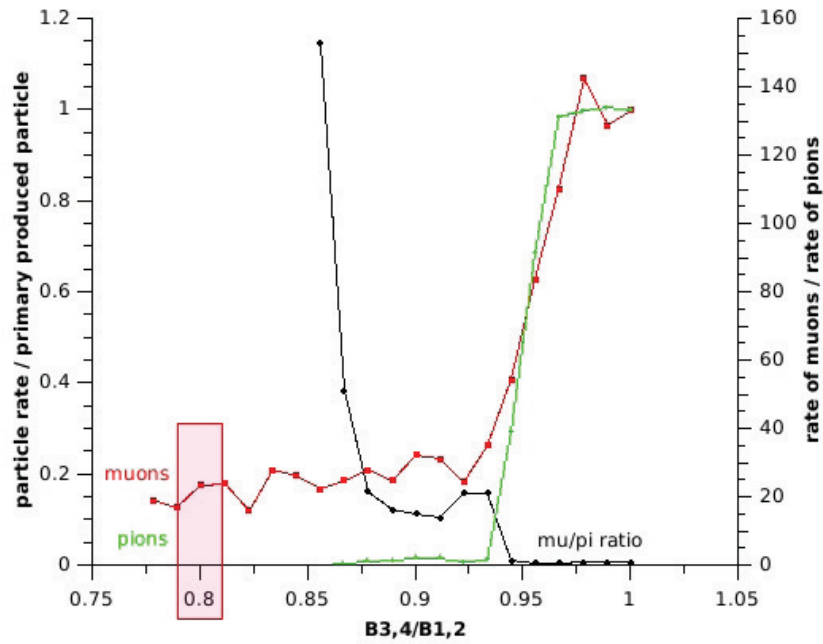
Figure 38: Number of muons μ (red), number of pions π (green), μ/π ratio (black) for 9 GeV/c out of a FLUKA simulation with varying magnet settings for the bending magnets B3 and B4.

Fluka **Simulations**

Top view of the geometry of the beam-line in Fluka (see Figs. 39 (Layout 1) and 40 (Layout 2)). The apertures of the magnets and the dump are made of iron. The cylindrical detector region ($\varnothing$ 30 cm) is placed 50 m downstream from the target. User-routines are used to count particles in the experimental area and to create the magnetic fields of the di- and quadrupole magnets. The following formulas are used:

Dipole magnets:

$$B0_{dipole}[\frac{\text{T}}{\text{cm}}] = \frac{\Theta[\text{mrad}] * p[\frac{\text{GeV}}{\text{c}}] * L[\text{m}]}{299.79} \tag{29}$$
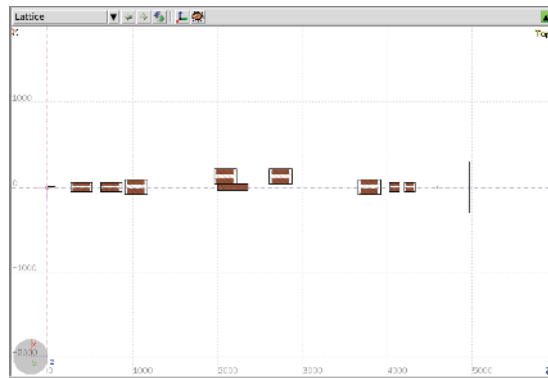
Figure 39: Top view of the Fluka Geometry Layout 1.
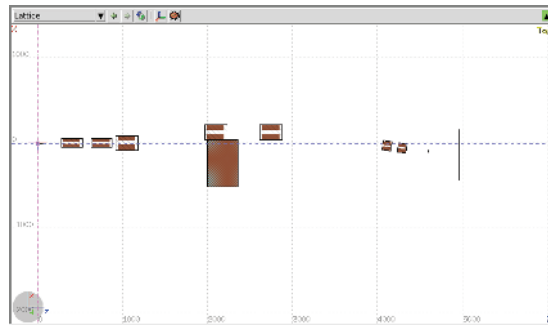
Figure 40: Top view of the Fluka Geometry Layout 2.

A muon beam-line simulation was made for initial 9 GeV π selected beam. The selection momentum for the muons is 7.2 GeV/c. The target in the simulation is a cylindrical 80 cm beryllium target with a radius of 2.5 cm. The number of simulated primary particles is 100000 with an initial momentum of 80 GeV/c. The apertures of the magnets and the beamdump for all simulations are made of iron.

Layout1
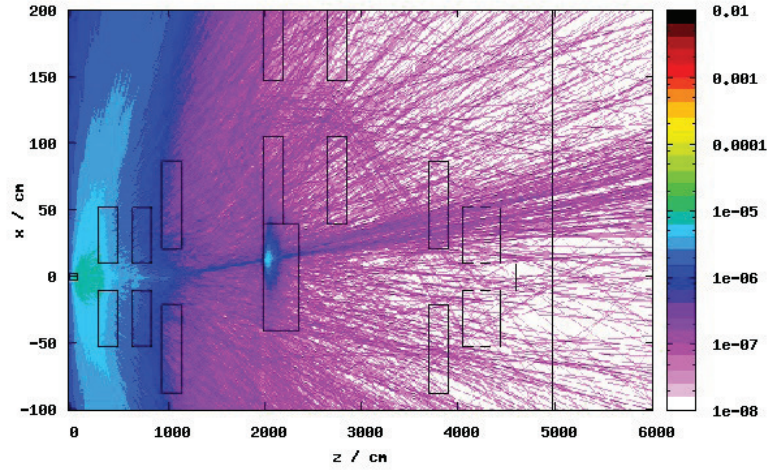
Figure 41: Muons of the low-energy muon beam of 9 GeV in the horizontal plane.
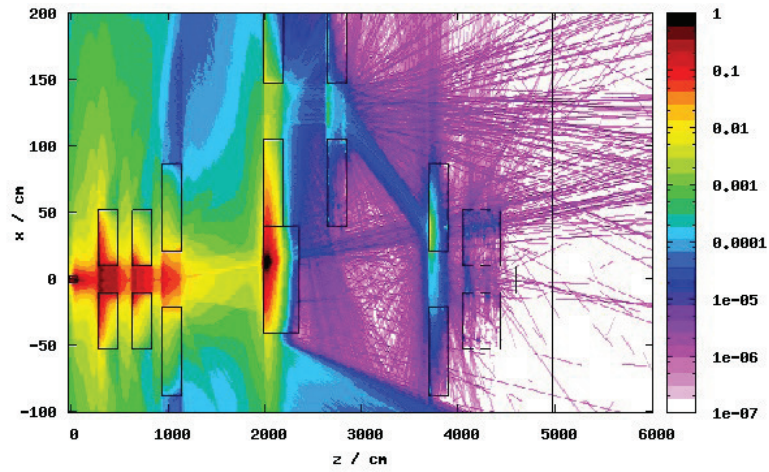
Figure 42: All particles of the low-energy muon beam of 9 GeV in the horizontal plane.
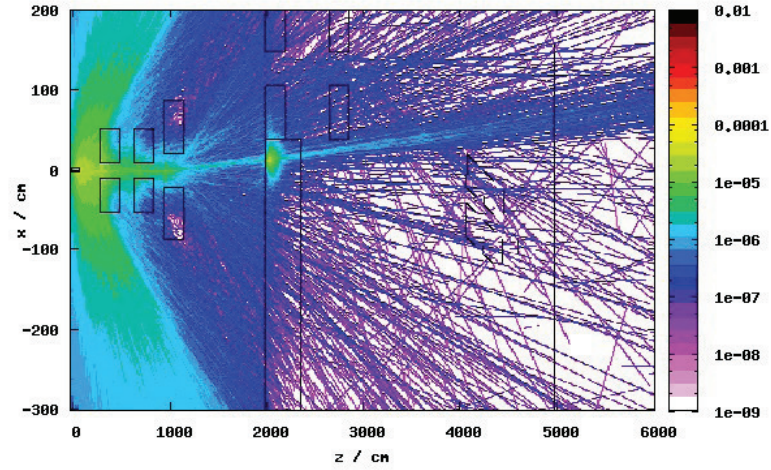
Layout 2

Figure 43: Muons of the low-energy pion beam of 9 GeV in the horizontal plane.
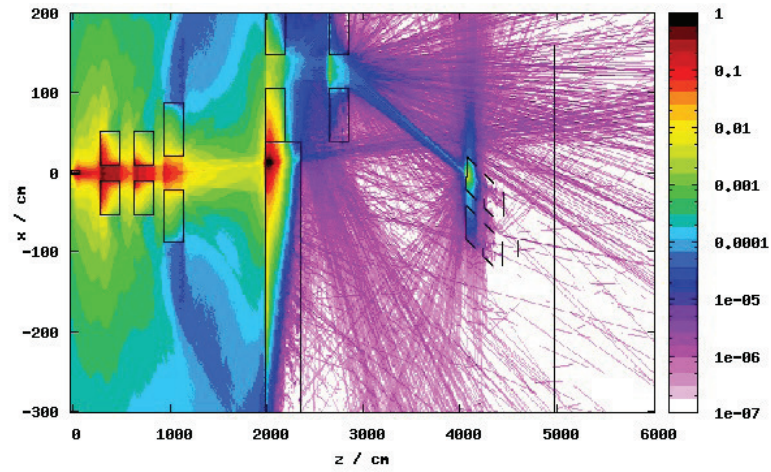
Figure 44: All particles of the low-energy pion beam of 9 GeV in the horizontal plane.

Table 6: Layout 1, simulation with 10^5 primary particles for the muon-beam.

Muon beam	μ	μ(Halo)	π^+	e^-	γ	n	μ^-	π^-
20 x 20	2	27	0	0	3	0	0	0
200 x 200	30	147	7	9	230	16	24	1
600 x 600	190	240	86	315	86127	1351	262	1019

Table 7: Layout 2, simulation with 10^5 primary particles for the muon-beam.

Muon beam	μ(Halo)	μ	π^+	p	π^-	e^+	γ	n	μ^-
20 x 20	0	3	0	0	0	0	7	0	0
200 x 200	8	21	4	3	1	8	170	80	36
600 x 600	234	164	66	286	80	211	44625	1547	218

3.4   Pion Beam Optimization

FLUKA simulation of the pion beam. As for the muon beam a 80 cm beryllium target with a radius of 2.5 cm is used for pion production. The number of simulated primary particles is 10000. The selection momentum is 9 GeV/c.
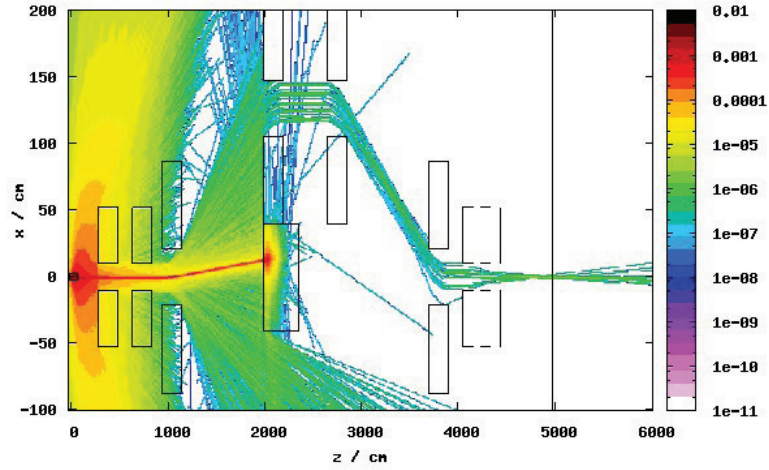
Layout 1

Figure 45: Pions of the low-energy pion beam of 9 GeV in the horizontal plane.
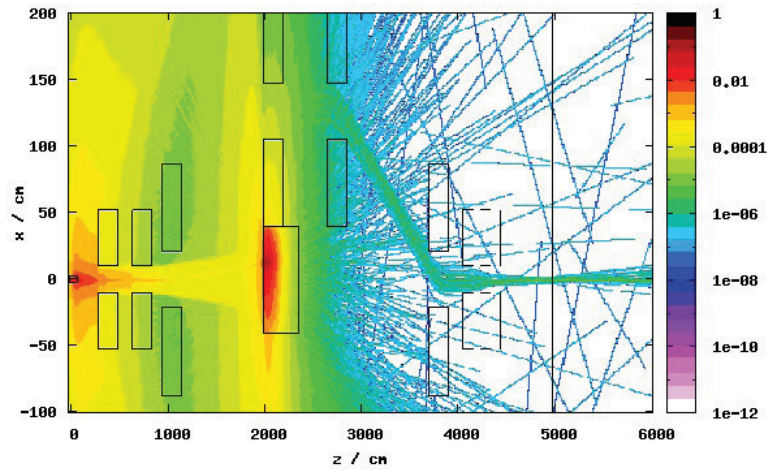
Figure 46: All particles of the low-energy pion beam of 9 GeV in the horizontal plane.

Layout 2
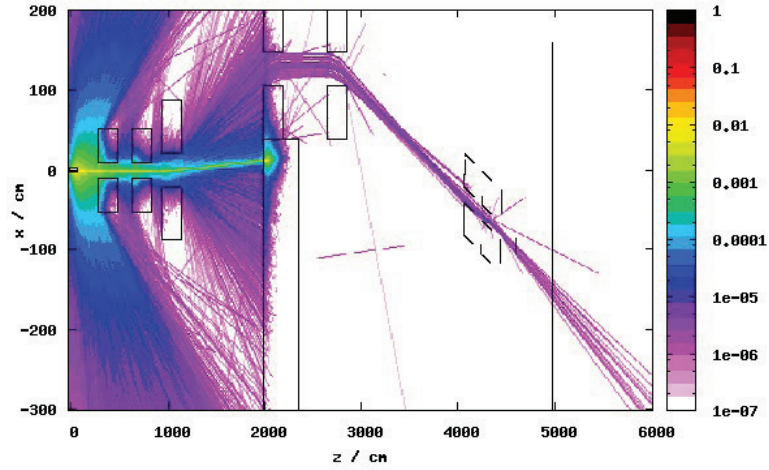
Figure 47: Pions of the low-energy electron beam of 9 GeV in the horizontal plane.

Figure 48: All particles of the low-energy electron beam of 9 GeV in the horizontal plane.
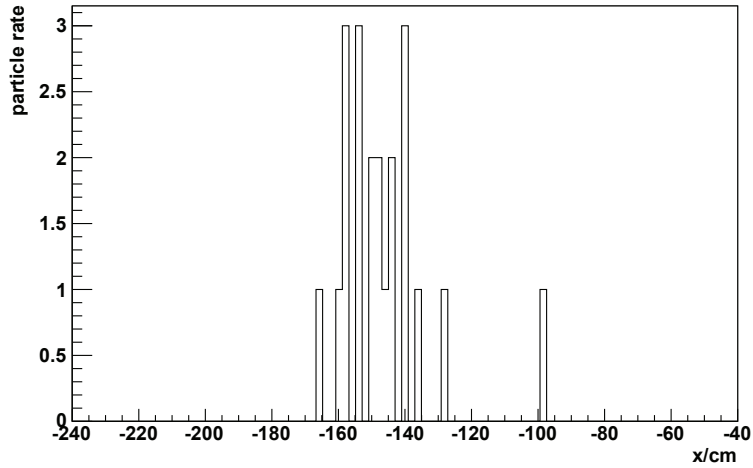
Figure 49: Example of the spot size of the pion beam in the horizontal plane for a simulation with layout 2.
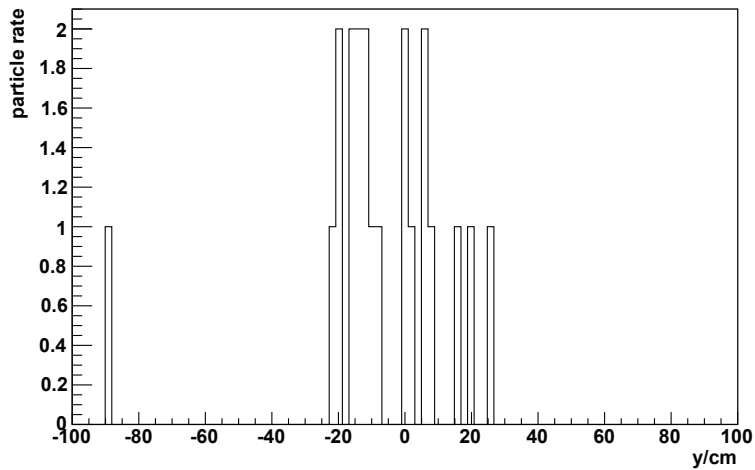
Figure 50: Example of the spot size of the pion beam in the vertical plane for a simulation with layout 2.

3.4.1 μ/π ratios

In order to get an idea of how many muons will be in the pion beam at the experiment, the number of muons and the number of pions was counted in a 10 x 10 cm and a 100 x 100 cm area with a TURTLE simulation. The number of muons and the number of pions was measured for different momentum settings of the beam-line. If the beam-line is set to select a momentum of 9 GeV/c the input beam was also produced with 9 GeV/c. The results can be seen in Figs. 51 and 52. As a first guess one can

43

say that around 2% (of the primary particles) muons will arrive at the experiment. The pion momentum loss is approximately 55 m/GeV.
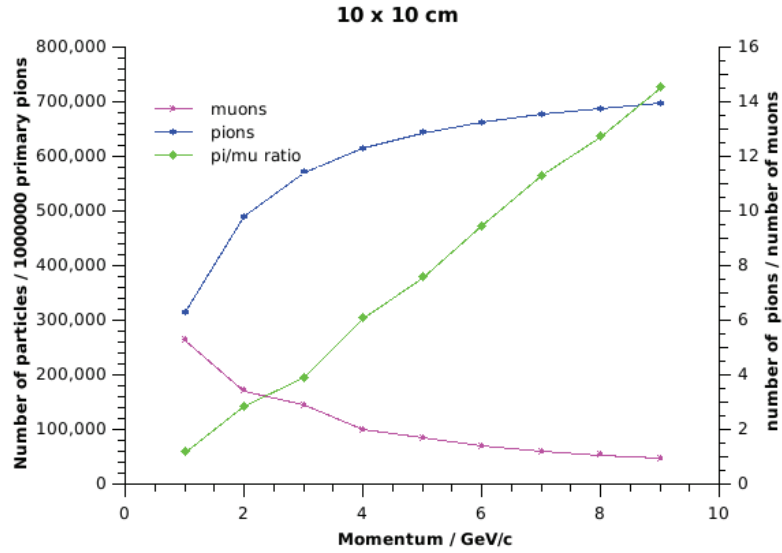
Figure 51: Number of pions (blue) and number of muons (pink) in 10 x 10 cm as a function of the momentum of the incoming beam.

Table 8: Layout 1, simulation with 10^4 primary particles for the pion beam.

Pion beam	μ	π^+	e^-	π^+ (Halo)	π^-	e^+	γ	n	μ^-	p
20 x 20	0	15	0	0	0	31	2	0	0	2
200 x 200	20	15	5	1	0	34	21	2	1	2
600 x 600	43	15	81	9	96	69	9456	134	26	7

Table 9: Layout 2, simulation with 10^4 primary particles for the pion beam.

Pion beam	μ	π^+	π^+(Halo)	p	e^+	γ	n	μ^-	$\bar{\pi}$
20 x 20	0	2	0	0	2	8	0	0	0
200 x 200	5	18	0	1	20	344	10	2	2
600 x 600	43	28	1	4	36	4875	164	17	8
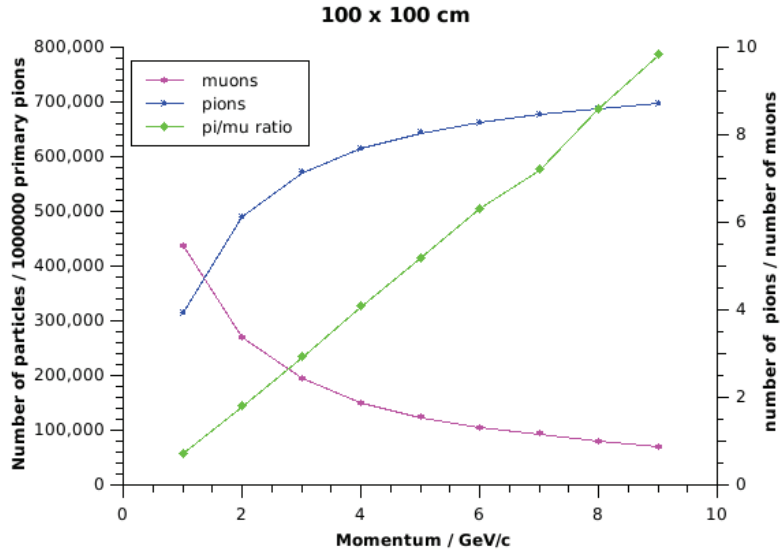
Figure 52: Number of pions (blue) and number of muons (pink) in 100 x 100 cm as a function of the momentum of the incoming beam.

3.5 Electron Beam Optimization

The FLUKA simulation of the electron beam uses a 2 cm ($\varnothing = 2.5$ cm) lead target. Since electrons carry a negative charge, the signs of the bending magnets are inverted. The magnetic settings are in principle the same as for the pion beam (see Tabs. 20, 19 and Figs. 16 and 15).

   The simulation procedure for the electrons is the same as for the pions, except that the Bremsstrahlung losses have to be considered and the magnetic settings should be corrected. But since the Bremsstrahlungsloss for electrons for one turn is:

$$U_0[\text{eV}] = 8.85 \cdot 10^4 \frac{E^4[\text{GeV}]}{\rho[\text{m}]} \tag{30}$$

$$\boxed{U_0[\text{eV}] = 2.65 \cdot 10^4 E^3[\text{GeV}]B[\text{T}]} \tag{31}$$

i.e. for 10 GeV:

$$U_0[\text{eV}] = 2.65 \cdot 10^4 \cdot 10^3 \cdot 1.8 = 4.77 \cdot 10^7 \,\widehat{=}\, 47.7 \text{ MeV} \tag{32}$$

≈ 50 MeV $\widehat{=}$ 0.05 GeV which is 0.5% of 10 GeV for a whole turn. In the beam-line the electrons will bend four times 120 mrad = $4 \cdot 0.12 = 0.48$ rad. A whole turn has $2 \cdot \pi \,\widehat{=}\, 6.283$ rad.

Therefore, the Bremsstrahlungsloss for the very-low energy extension can be estimated to:

$$U_0 = 3.8 \text{ MeV} \tag{33}$$

which is roughly 0.04% of 10 GeV and therefore smaller than the accuracy of the power supply of the magnets and negligible.

The FLUKA simulation of the electron uses a 2.0 cm lead target for low-energy electron production. The selection momentum is 9 GeV/c.
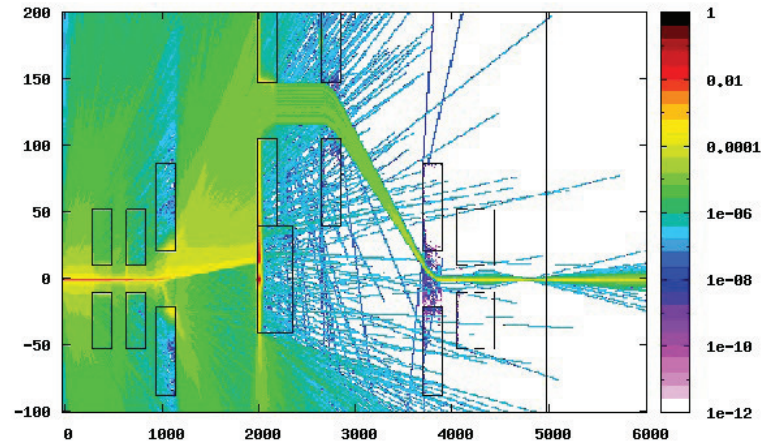
Layout1

Figure 53: Electrons of the low-energy electron beam of 9 GeV in the horizontal plane.
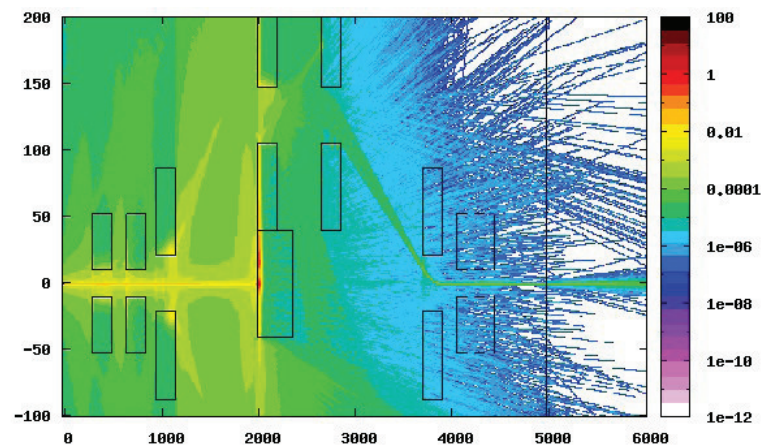
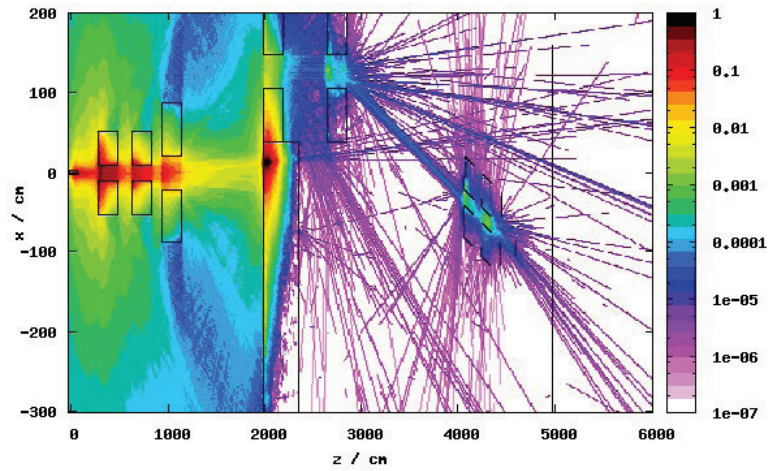Figure 54: All particles of the low-energy electron beam of 9 GeV in the horizontal plane.
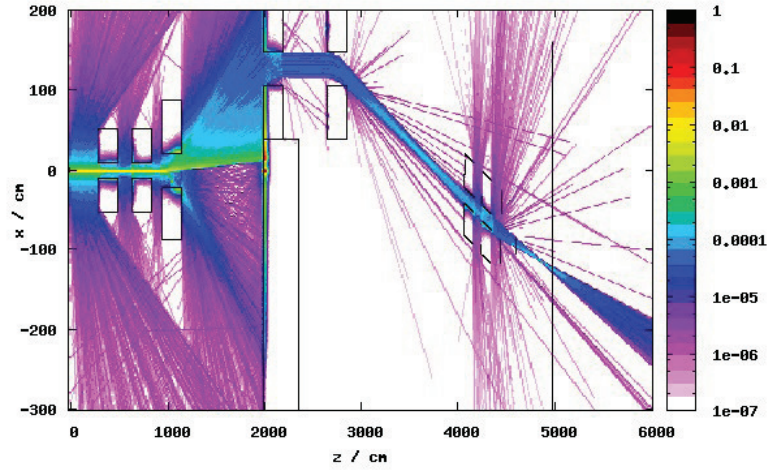
Layout 2

Figure 55: Electrons of the low-energy electron beam of 9 GeV in the horizontal plane.
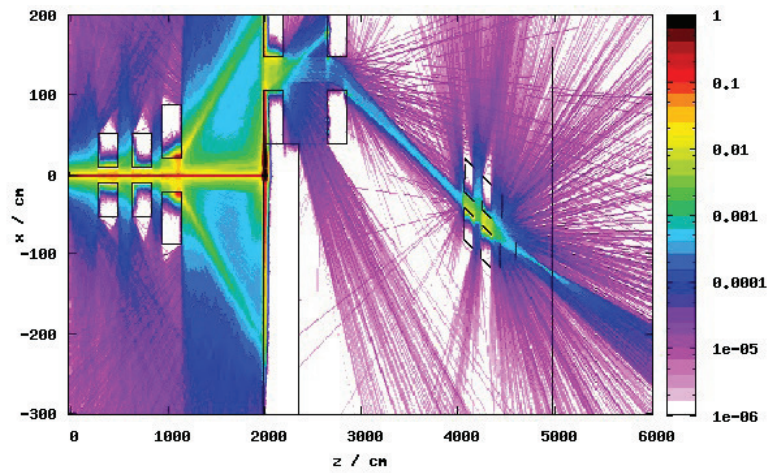
Figure 56: All particles of the low-energy electron beam of 9 GeV in the horizontal plane.

Table 10: Layout 1, simulation with 10^4 primary particles for the electron beam.

Electron beam	μ	π^+	e^-	γ	μ^-	π^-	e^+
20 x 20	0	0	744	0	0	0	0
200 x 200	0	0	756	33	0	0	0
600 x 600	0	0	863	3480	0	0	694

Table 11: Layout 2, simulation with 10^4 primary particles for the electron beam.

Electron beam	μ	e^-	γ	e^+	e^-(Halo)
20 x 20	0	368	145	0	0
200 x 200	0	392	3959	16	8
600 x 600	0	462	10676	120	78
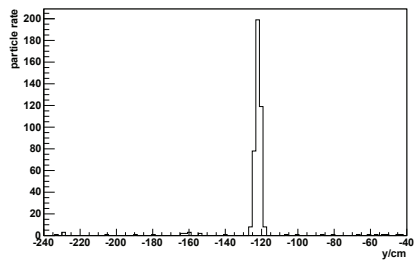
Figure 57: Example of the spot size of the electron beam in the horiz. plane for a simulation with layout 2.
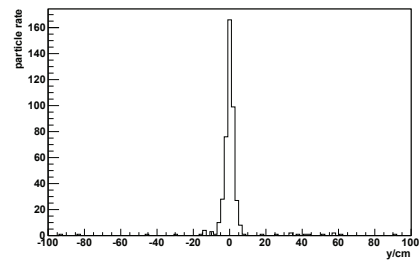
Figure 58: Example of the spot size of the electron beam in the vert. plane for a simulation with layout 2.

4   Beam to Experiment

4.1   Background

The high energy muons produced before the secondary target will travel through the beam-line with only very few interactions and the high energy muons will arrive at the experiment. A FLUKA simulation of a 72 ± 3 GeV/c muon beam with a beam size of 1 m^2 (estimated high energy muon background coming from the primary target) shows Fig. 59. With layout option 2 most of these unwanted muons won't reach the experiment.
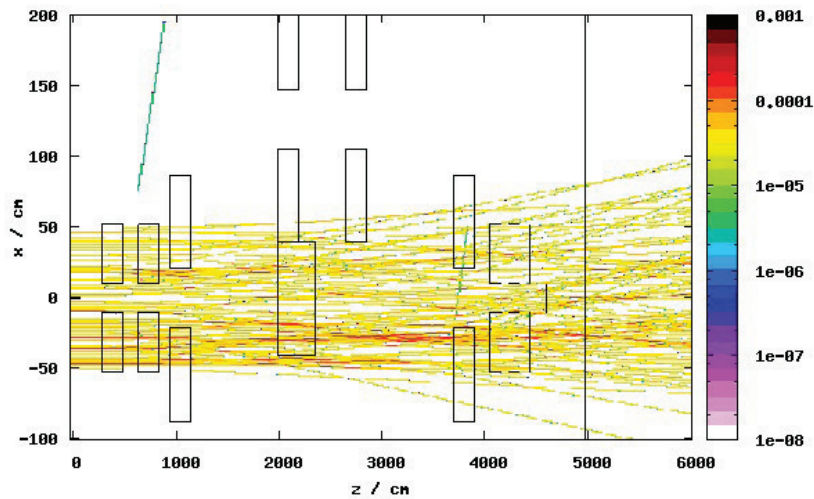
Figure 59: 1 m^2, 72 ± 3 GeV/c muon beam traveling through the beam-line (layout 1).

5   Summary

This beam-line is able to provide 1-9 GeV/c pions, muons and electrons. Two basic layout options were studied. Layout 1 (see Fig. 11) with four bending magnets and the experiment at the central line, and layout 2 (see Fig. 12) with three bending magnets and the experiment off-axis.

The optics for the beam-line were optimized with TRANSPORT and TURTLE and are shown in Figs. 13 to 16.

FLUKA simulations were done in order to optimize the beam-line and to get the particle rates at the experiment for the muon pion and electron beams. The data for both layouts are summarized in Tabs. 12 and 13.

Layout option 2 gives as expected a purer muon beam with less background.

Table 12: Layout 1, simulation with 10^5 primary particles for the muon and 10^4 for the pion and electron beam.
* Halo-particle

Muon	μ	μ^*	π^+	e^-	γ	n	μ^-	π^-		
20 x 20	2	27	0	0	3	0	0	0		
200 x 200	30	147	7	9	230	16	24	1		
600 x 600	190	240	86	315	86127	1351	262	1019		
Pion	μ	π^+	e^-	π^{+*}	π^-	e^+	γ	n	μ^-	p
20 x 20	0	15	0	0	0	31	2	0	0	2
200 x 200	20	15	5	1	0	34	21	2	1	2
600 x 600	43	15	81	9	96	69	9456	134	26	7
Electron	μ	π^+	e^-	γ	μ^-	π^-	e^+			
20 x 20	0	0	744	0	0	0	0			
200 x 200	0	0	756	33	0	0	0			
600 x 600	0	0	863	3480	0	0	694			

51

Table 13: Layout 2, simulation with 10^5 primary particles for the muon and 10^4 for the pion and electron beam.

* Halo-particle

Muon	μ^*	μ	π^+	p	π^-	e^+	γ	n	μ^-
20 x 20	0	3	0	0	0	0	7	0	0
200 x 200	8	21	4	3	1	8	170	80	36
600 x 600	234	164	66	286	80	211	44625	1547	218
Pion	μ	π^+	π^{+*}	p	e^+	γ	n	μ^-	$\bar{\pi}$
20 x 20	0	2	0	0	2	8	0	0	0
200 x 200	5	18	0	1	20	344	10	2	2
600 x 600	43	28	1	4	36	4875	164	17	8
Electron	μ	e^-	γ	e^+	e^{-*}				
20 x 20	0	368	145	0	0				
200 x 200	0	392	3959	16	8				
600 x 600	0	462	10676	120	78				

Appendix

Appendix I - Simulated Beam Rates

Table 14: Scanning through the bending magnets for different selection energies. The number of muons and pions arriving at the experiment and the $\frac{\mu}{\pi}$ ratio for an initial momentum of 9 GeV/c.

$|p|$ is the initial momentum of the particles, B_i the strength of bending magnet number i, μ the total number of muons, π the total number of pions, and $\frac{\mu}{\pi}$ the muon to pion ratio at the experiment.

$|p|/\frac{\text{GeV}}{\text{c}}$	$-B_1, B_2/\text{T}$	$B_3, -B_4/\text{T}$	μ	π	$\frac{\mu}{\pi}$
9.0	1.801	1.801	272	9026	0.030
8.9	1.801	1.781	263	9076	0.029
8.8	1.801	1.761	291	9015	0.032
8.7	1.801	1.741	225	8879	0.025
8.6	1.801	1.721	171	6198	0.027
8.5	1.801	1.701	111	2655	0.041
8.4	1.801	1.681	72	113	0.630
8.3	1.801	1.661	50	78	0.641
8.2	1.801	1.641	64	152	0.421
8.1	1.801	1.621	66	145	0.455
8.0	1.801	1.601	51	103	0.495
7.9	1.801	1.581	57	87	0.655
7.8	1.801	1.561	51	33	1.545
7.6	1.801	1.541	46	10	4.600
7.5	1.801	1.521	54	0	-
7.4	1.801	1.501	57	0	-
7.3	1.801	1.481	33	0	-
7.2	1.801	1.461	49	0	-
7.1	1.801	1.441	48	0	-
7.0	1.801	1.421	35	0	-

Table 15: Scanning through the bending magnets for different selection energies. The number of muons and pions arriving at the experiment and the $\frac{\mu}{\pi}$ ratio for an initial momentum of 6 GeV/c.

$|p|$ is the initial momentum of the particles, B_i the strength of bending magnet number i, μ the total number of muons, π the total number of pions, and $\frac{\mu}{\pi}$ the muon to pion ratio at the experiment.

$|p|/\frac{\text{GeV}}{\text{c}}$	$-B_1, B_2/\text{T}$	$B_3, -B_4/\text{T}$	μ	π	$\frac{\mu}{\pi}$
6.0	1.201	1.201	326	8626	0.037
5.9	1.201	1.181	330	8618	0.038
5.8	1.201	1.161	230	8146	0.028
5.7	1.201	1.141	199	4053	0.049
5.6	1.201	1.121	76	161	0.472
5.5	1.201	1.101	71	95	0.747
5.4	1.201	1.081	73	103	0.695
5.3	1.201	1.061	66	62	1.064
5.2	1.201	1.041	61	21	2.904
5.1	1.201	1.021	46	3	15.33
5.0	1.201	1.001	42	0	-
4.9	1.201	0.981	44	0	-
4.8	1.201	0.961	27	0	-
4.7	1.201	0.941	42	0	-
4.6	1.201	0.921	42	0	-
4.5	1.201	0.901	27	0	-
4.4	1.201	0.881	19	0	-
4.3	1.201	0.861	27	0	-
4.2	1.201	0.841	23	0	-
4.1	1.201	0.821	16	0	-

Table 16: Scanning through the bending magnets for different selection energies. The number of muons and pions arriving at the experiment and the $\frac{\mu}{\pi}$ ratio for an initial momentum of 15 GeV/c.
$|p|$ is the initial momentum of the particles, B_i the strength of bending magnet number i, μ the total number of muons, π the total number of pions, and $\frac{\mu}{\pi}$ the muon to pion ratio at the experiment.

$|p|/\frac{\text{GeV}}{\text{c}}$	$-B_1, B_2/\text{T}$	$B_3, -B_4/\text{T}$	μ	π	$\frac{\mu}{\pi}$
15.0	3.002	3.002	191	9405	0.020
14.9	3.002	2.982	188	9422	0.019
14.8	3.002	2.962	191	9435	0.020
14.7	3.002	2.942	175	9408	0.018
14.6	3.002	2.922	173	9438	0.018
14.5	3.002	2.902	164	9442	0.017
14.4	3.002	2.882	153	8915	0.017
14.3	3.002	2.862	114	6062	0.018
14.2	3.002	2.842	83	2657	0.031
14.1	3.002	2.822	45	170	0.264
14.0	3.002	2.802	47	1	47
13.9	3.002	2.782	46	12	3.833
13.8	3.002	2.762	41	52	0.788
13.7	3.002	2.742	45	153	0.294
13.6	3.002	2.722	44	208	0.211
13.5	3.002	2.702	38	273	0.139
13.4	3.002	2.682	45	238	0.189
13.3	3.002	2.662	47	249	0.188
13.2	3.002	2.642	28	165	0.169
13.1	3.002	2.622	41	105	0.390
13.0	3.002	2.602	35	74	0.472
12.9	3.002	2.582	33	39	0.846
12.8	3.002	2.562	35	11	3.181
12.7	3.002	2.542	44	1	44.00
12.6	3.002	2.522	35	1	35.00
12.5	3.002	2.502	34	2	17.00
12.4	3.002	2.482	32	1	32.00
12.3	3.002	2.462	27	0	-
12.2	3.002	2.442	41	0	-
12.1	3.002	2.422	34	1	34.00
12.0	3.002	2.402	41	0	-

Appendix II - Magnet Settings and Positions of the Elements

Table 17: Magnetic field strengths for the bending magnets for various energies.
$|p|$ is the initial momentum of the primary particles in GeV/c, B is the magnetic field in Tesla, B_μ is 80 % of the initial magnetic field for the muon beam-line and $|p|_\mu$ 80 % of the initial momentum for the muon beam-line in GeV/c.

$|p|_\pi/$GeV/c	$B_\pi/$T	$|p|_\mu/$GeV/c	$B_\mu/$T
10	2.0	8.0	1.60
9	1.8	7.2	1.44
8	1.6	6.4	1.28
7	1.4	5.6	1.12
6	1.2	4.8	0.96
5	1.0	4.0	0.80
4	0.8	3.2	0.64
3	0.6	2.4	0.48
2	0.4	1.6	0.32
1	0.2	0.8	0.16

Table 18: Magnetic settings for the quadrupole magnets for the muon beam for different energies. $|p|$ is the initial momentum of the pions, $|p|_{muon}$ the momentum of the muons ($|p|_{muon} = 0.8 * Mom$) and Q_i the strength of quadrupole magnet number i.

$|p|/\frac{GeV}{c}$	$Q_1/\frac{T}{m}$	$Q_2/\frac{T}{m}$	$|p|_{muon}/\frac{GeV}{c}$	$Q_3/\frac{T}{m}$	$Q_4/\frac{T}{m}$
15	-10.688	5.666	12.0	-11.453	14.911
14	-9.975	5.288	11.2	-10.689	13.917
13	-9.263	4.911	10.4	-9.926	12.923
12	-8.550	4.533	9.6	-9.162	11.929
11	-7.838	4.155	8.8	-8.399	10.953
10	-7.125	3.777	8.0	-7.635	9.941
9	-6.413	3.400	7.2	-6.872	8.947
8	-5.700	3.022	6.4	-6.108	7.952
7	-4.987	2.644	5.6	-5.344	6.958
6	-4.275	2.266	4.8	-4.581	5.964
5	-3.562	1.888	4.0	-3.817	4.976
4	-2.850	1.511	3.2	-3.054	3.976
3	-2.137	1.133	2.4	-2.290	2.982
2	-1.425	0.755	1.6	-1.527	1.988
1	-0.413	0.377	0.8	-0.763	0.994

Table 19: Magnetic settings for the quadrupole magnets for the pion and electron beam and 4 bending magnets for different energies. $|p|$ is the momentum of the particles and Q_i the strength of quadrupole magnet number i.

$|p|/\text{GeV}$	$Q_1/\frac{\text{T}}{\text{m}}$	$Q_2/\frac{\text{T}}{\text{m}}$	$Q_3/\frac{\text{T}}{\text{m}}$	$Q_4/\frac{\text{T}}{\text{m}}$
15	-10.688	5.153	13.153	-17.416
14	-9.975	4.809	12.276	-16.255
13	-9.263	4.466	11.399	-15.094
12	-8.550	4.122	10.522	-13.933
11	-7.838	3.779	9.645	-12.772
10	-7.125	3.435	8.768	-11.611
9	-6.413	3.092	7.892	-10.450
8	-5.700	2.748	7.015	-9.288
7	-4.987	2.404	6.138	-8.127
6	-4.275	2.061	5.261	-6.966
5	-3.562	1.717	4.384	-5.805
4	-2.850	1.374	3.507	-4.644
3	-2.139	1.030	2.630	-3.483
2	-1.425	0.687	1.753	-2.322
1	-0.712	0.343	0.876	-1.161

Table 20: Magnetic settings for the quadrupole magnets for the pion and electron beam and 3 bending magnets for different energies. $|p|$ is the momentum of the particles and Q_i the strength of quadrupole magnet number i.

Mom/GeV/c	Q1$/\frac{\text{T}}{\text{m}}$	Q2$/\frac{\text{T}}{\text{m}}$	Q3$/\frac{\text{T}}{\text{m}}$	$Q4/\frac{\text{T}}{\text{m}}$
15	-10.688	5.153	13.665	-17.695
14	-9.975	4.809	12.754	-16.515
13	-9.263	4.466	11.843	-15.335
12	-8.550	4.122	10.932	-14.156
11	-7.838	3.779	10.021	-12.976
10	-7.125	3.435	9.110	-11.796
9	-6.413	3.092	8.199	-10.617
8	-5.700	2.748	7.288	-9.437
7	-4.987	2.404	6.377	-8.257
6	-4.275	2.061	5.466	-7.078
5	-3.562	1.717	4.555	-5.898
4	-2.850	1.374	3.644	-4.718
3	-2.137	1.030	2.733	-3.539
2	-1.425	0.687	1.822	-2.359
1	-0.712	0.343	0.911	-1.179

Table 21: Positions and type of the magnets. Z_1 and Z_2 are the longitudinal Z-positions of the elements for the two designs.

Name	Z_1/cm	Z_2/cm	Type
Quad1	300	300	QPL
Quad2	650	650	QPL
Bend1	950	950	MBPL
Bend2	2000	2000	MBPL
Bend3	2650	2650	MBPL
Bend4	3700	-	MBPL
Quad3	4050	4050	QPS
Quad4	4230	4230	QPS
Solenoid	4480	4480	Morpurgo
Experiment	4970	4970	

References

[1] AIDA MIND and TASD project

[2] CERN

[3] Transport, A Computer Program for Designing Charged Particle Beam Transport Systems, K.L. Brown, D.C. Carey, Ch. Iselin, F. Rothacker, Geneva 1980 CERN 80-04 Super Proton Synchrotron Division

[4] Turtle$^+$ (Trace Unlimited Rays Through Lumped Elements) F. Attallah, J.F Chemin, J.N. Scheurer, Centre d'Etudes Nucleaires de Bordeaux-Gradignan,1994

[5] HALO, A Computer Program to Calculate Muon Halo, Ch. Iselin, Geneva 1974, CERN 74-17

[6] Fluka, A multi-particle transport code, Program version 2011, A. Ferrari, P. Sala, A. Fasso, J. Ranft, Geneva 2011, CERN-2005-010, INFN TC05/11 SLAC-R-773, 12 October 2005

[7] Particle Beams for FT Experiments,I. Efthymiopoulos - CERN - EDMS No: 1165938 CAS - Chios

[8] An Indroduction to the Design of High-Energy Charged Particle Beams, P. Coet N. Doble, Prevessin September 1986, CERN/SPS/86-23 (EBS)

[9] CAS CERN Accelerator School, Fifth General Accelerator Physics Course, CERN 94-01 26 January 1994 Vol. I, Editor: S. Turner

[10] ROOT, An Object-Oriented Data Analysis Framework Users Guide, http://root.cern.ch/drupal/content/users-guide

[11] J. Beringer et al. (Particle Data Group), Phys. Rev. D86, 010001 (2012) and 2013 partial update for the 2014 edition.